

Spectral features of tidal-disruption candidates and alternative origins for such transient flares

Curtis J. Saxton,^{*} Hagai B. Perets & Alexei Baskin[†]

Physics Department, Technion - Israel Institute of Technology, Haifa, Israel 3200002

Accepted 2017 November 08. Received 2017 November 08 ; in original form 2016 December 21

ABSTRACT

UV and optically selected candidates for stellar tidal disruption events (TDE) often exhibit broad spectral features (He II emission, H α emission, or absorption lines) on a blackbody-like continuum ($10^4\text{K} \lesssim T \lesssim 10^5\text{K}$). The lines presumably emit from TDE debris or circumnuclear clouds photoionized by the flare. Line velocities however are much lower than expected from a stellar disruption by supermassive black hole (SMBH), and are somewhat faster than expected for the broad line region (BLR) clouds of a persistently active galactic nucleus (AGN). The distinctive spectral states are not strongly related to observed luminosity and velocity, nor to SMBH mass estimates. We use exhaustive photoionization modelling to map the domain of fluxes and cloud properties that yield (e.g.) a He-overbright state where a large He II(4686Å)/H α line-ratio creates an illusion of helium enrichment. Although observed line ratios occur in a plausible minority of cases, AGN-like illumination can not reproduce the observed equivalent widths. We therefore propose to explain these properties by a light-echo photoionization model: the initial flash of a hot blackbody (detonation) excites BLR clouds, which are then seen superimposed on continuum from a later, expanded, cooled stage of the luminous source. The implied cloud mass is substellar, which may be inconsistent with a TDE. Given these and other inconsistencies with TDE models (e.g. host-galaxies distribution) we suggest to also consider alternative origins for these nuclear flares, which we briefly discuss (e.g. nuclear supernovae and starved/subluminous AGNs).

Key words: accretion, accretion discs — black hole physics — galaxies: active — galaxies: nuclei — quasars: emission lines

1 INTRODUCTION

Early theorists considered that active galactic nuclei (AGN) and quasars might consist of a supermassive black hole (SMBH, of mass m_\bullet) accreting gas derived from the tidal disruption of stars in the nuclear cluster (Hills 1975; Frank & Rees 1976; Young, Shields & Wheeler 1977; Ozernoi & Reinhardt 1978; Kato & Hōshi 1978). A star of mass m_\star and radius R_\star disrupts if it passes within the ‘tidal radius,’ $R_t = R_\star(m_\bullet/m_\star)^{1/3}$. The consequences would be similar if the nucleus hosts any other sufficiently dense and relativistic type of dark supermassive object (e.g. Goel et al. 2015; Meliani et al. 2015; Saxton, Younsi & Wu 2016). Larger SMBH ($m_\bullet \gtrsim \text{few} \times 10^8 m_\odot$) can swal-

low main sequence stars whole, without a tidal disruption event (TDE). The TDE rate needed to power AGN turned out to be difficult to reconcile with stellar densities, at least in the nuclei of modern galaxies (and gas accretion now seems more important to AGN). Nonetheless it was recognized that a TDE could produce a distinctive flare, peaking in much less than a year and potentially remaining observable during a few years of fading (Lidskii & Ozernoi 1979; Gurzadian & Ozernoi 1981; Lacy, Townes & Hollenbach 1982; Luminet & Marck 1985; Rees 1988). TDEs by lower mass SMBHs ($m_\bullet \lesssim 3 \times 10^7 m_\odot$) are more likely to accrete at rates exceeding the Eddington (1918) radiation pressure limit (Ulmer 1999).

More than ten transient events detected in ultraviolet and optical (UV/O), X-ray and γ -ray monitoring and serendipitous observations are currently classified as TDE candidates (Komossa 2015). These were selected for their central locations in the host galaxies. Candidates are usually excluded if the host showed conventional signatures of an AGN (in spectroscopy, variability, and radio counterparts)

^{*} E-mail: saxton@physics.technion.ac.il (CJS);

hperets@physics.technion.ac.il (HBP);

alexei@physics.technion.ac.il (AB);

[†] Present address: Soreq Nuclear Research Center, Yavne 8180000, Israel

before and long after the transient¹. The relation between TDE candidates observed as γ -ray/X-ray flares and those detected in the UV/O is not yet clear. We note that much smaller, stellar black holes, may also tidally disrupt stars. These would lead to μ TDEs which might resemble ultra-long γ -ray bursts/X-ray flares and jetted-TDE candidates (Perets et al. 2016), but not the UV/O TDE-candidates on which we focus here.

Arcavi et al. (2014) classified the UV/O candidates into a sequence by their broad line spectral states: He-overbright cases; some with He II and H α ; and others with H α dominating. PS1-11af had broad absorption lines (beyond the scope of our emission modelling) but it is notable that the velocity widths were comparable to velocity widths of emission-line TDE candidates (Chornock et al. 2014). We note that Drake et al. (2011) classified another transient (in a Seyfert host with prior radio detection) as an exotic supernova rather than a TDE, partly because the temperature was below predictions of early TDE theories. We disagree with this exclusion, since the properties were actually consistent with more recent UV/O TDE candidates, and suggest to include this as an additional TDE candidate (for our table of currently identified UV/O TDE-candidates, see the Appendix A). Although spectroscopic observations have been sparse in time, a few UV/O events have evolved from one emission line state to another. Our paper will study the spectroscopic features of TDE candidates, and analyse them using detailed photoionization models.

Previous studies by Gaskell & Rojas Lobos (2014) and Guillochon, Manukian & Ramirez-Ruiz (2014) tried to explain the spectral features of the UV/O TDE candidates. However, as we show in the following, none of the simple models suggested in the literature, typically involving AGN-like illumination, can actually explain the spectral properties of the candidates. In particular, though the line-ratios can be explained by models as suggested by Guillochon, Manukian & Ramirez-Ruiz (2014) and Gaskell & Rojas Lobos (2014), they fail to explain the *observed* equivalent width. We suggest a model which may overcome these difficulties, and provide novel predictions for the spectral temporal evolution. We consider how states similar to the observed line ratios and equivalent widths can arise in generic models of TDE, AGN outbursts, and other explosive events. Using models of photoionized spectra, we distinguish among luminous source spectra that can reproduce the observed lines.

Besides the failure of the simple picture to explain the observed spectral features, our current interpretation of candidate TDEs as bona-fide ‘real’ TDEs encounters several other difficulties. We complement our photoionization modeling with an analysis of these additional challenges and their implications, and briefly discuss other possible origins for the observed TDE candidates.

Our paper is organized as follows. We begin by describing our modeling of the spectral features of TDEs in Section 2, and show that none of the simple models can explain both the line ratios and equivalent widths seen in observations. We propose a novel model which could potentially

resolve these difficulties (Section 2.2), and then discuss our results as well the possible origins of such nuclear flares (Section 3), and in particular possible alternatives to the TDE origin, including subluminal AGN flaring and nuclear supernovae (Section 3.3.1).

2 MODELING

The principal luminous media in a TDE include the dense tidal stream of bound debris, which orbits round to shock its own tail and form an accretion disc; unbound debris escaping the system ballistically; and a radiation-driven wind. If the TDE continuum emission photoionizes circumnuclear gas clouds, like those of AGN, their line emissions may resemble an AGN’s broad emission line regions (BLRs) except evolving on shorter time-scales. For the moment, we are agnostic about whether the luminous source originated as a TDE or some other type of transient event. (It is also unimportant whether the clouds originated from the flare, or already orbited dormant in the inner galaxy.) In the following, we model the expected spectral features, and compare them with the observed features. We find that current models are inconsistent with observed features, and we discuss a novel echo model that could be reconciled with observations.

2.1 Emission line ratios and equivalent widths

To interpret observations, we require predictions of both the He II(4686Å) and H α (6563Å) intensities, as well as the line ratios, the underlying continuum, and other lines that might appear. These synthetic observables are generic and time-independent: they should apply equally to slowly evolving structure under variable illumination (e.g. BLR during an AGN flare) or dynamically evolving clouds under a steady or variable radiation source (e.g. TDE debris). In order to do so, our calculations (below) follow photoionization models employing the CLOUDY code (Ferland et al. 2013). The standard approach (Baldwin et al. 1995; Korista & Goad 2004) is to compute emission line output of clouds across the ‘flux-density plane’, $(n_{\text{H}}, \Phi_{\text{H}})$, where n_{H} is the cloud density, and Φ_{H} is ionizing flux from an isotropic source with a specified spectral energy distribution (SED), given by

$$\Phi_{\text{H}} = \frac{L}{4\pi r^2 \bar{\epsilon}}, \quad (1)$$

where $\bar{\epsilon}$ is an effective mean ionizing photon energy for the given SED.

As calculated by Guillochon, Manukian & Ramirez-Ruiz (2014) and Gaskell & Rojas Lobos (2014), emission line ratios consistent with the He II-overbright state are attainable in specific cloud conditions, though they considered an AGN SED model of Mathews & Ferland 1987 (hereafter ‘MF1987’); moreover, see Strubbe & Murray 2015 for different conclusions). However, the observed ratios are a necessary but not *sufficient* constraint; any successful model should also provide the correct *equivalent widths* of the lines. As we show in the following, *all* the models, and in particular current SED models (constructed to be consistent with observations), on which we focus thus far fail to produce both the line ratios and the equivalent widths

¹ Realistically, TDE could just as well occur around active nuclei, but observers prefer to avoid false-positive identifications.

(but this is also true for the MF1987 model, considered here only for comparison with previous works).

If the line intensity emerging from a cloud is I_{line} and the incident continuum is F_{λ} , the equivalent width (‘EW’) is $W_{\lambda} \equiv I_{\text{line}}/F_{\lambda}$. The integrated EW of a composite system depends on the covering fraction of the clouds, Ω . Observationally, emission lines with $W_{\lambda} < 1\text{\AA}$ might be undetectable. Gezari et al. (2012), observing PS1-10jh, found an He II line luminosity of $(9 \pm 1) \times 10^{40} \text{erg s}^{-1}$, which corresponds to $W_{4686} = 66.4 \pm 13.9\text{\AA}$; while van Velzen et al. (2011) report a H α value $W_{6563} = 87 \pm 5\text{\AA}$ for TDE2. The He II-overbright early state of ASASSN-15oi had an equivalent width $W_{4686} = 99 \pm 13\text{\AA}$ (Holoien et al. 2016a). By visual inspection, other UV/O candidates’ broad lines typically have equivalent widths of similar order (Wang et al. 2011; Drake et al. 2011; Holoien et al. 2014; Arcavi et al. 2014). These facts require models of the continuum and clouds that provide W_{λ} of at least a few \AA , for some covering factor. Therefore, models predicting smaller W_{λ} values for a full coverage are not viable matches for known UV/O transients, even if the line-ratios match.

Previous calculations (Gaskell & Rojas Lobos 2014; Guillochon, Manukian & Ramirez-Ruiz 2014) allowed a spatially extensive line-emitting medium, analogous to the BLR of an AGN, and employed the AGN-like MF1987 SED model. This SED model is inconsistent with observed AGN SEDs (Laor et al. 1997, and citations thereafter). Gaskell & Rojas Lobos (2014) and Guillochon, Manukian & Ramirez-Ruiz (2014) find that the He-overbright state (e.g. with the line ratio $w \equiv I_{4686}/I_{6563} \approx 4$ observed in PS1-10jh) occurs naturally in specific photoionization conditions, without requiring helium-enriched gas. Guillochon, Manukian & Ramirez-Ruiz (2014) obtained time-dependent functions of $(n_{\text{H}}, \Phi_{\text{H}})$ from hydrodynamic simulations of TDE streams, and showed that these tracks cross a He-overbright region of the flux-density plane (at least when the column $N_{\text{H}} = 10^{23} \text{cm}^{-2}$ exactly).

Roth et al. (2016) performed radiative transfer simulations of a TDE’s opaque quasi-spherical outflow, with a prescribed density profile, resulting in line emission (at an assumed velocity width) escaping from layers near the continuum source’s photosphere. He II-overbright states with $EW \gtrsim 100\text{\AA}$ (by inspection of their figures) appeared naturally in some configurations with outer radii $\leq 2 \times 10^{15} \text{cm}$. Are these conditions special, or commonplace, and do they persist as the source evolves? In their model, the line emission depends on the properties of the entire surface ($\Omega = 1$) and layers beneath. We might wonder whether the photosphere’s compactness would lead to significant intra-day spectral variability.

In our paper, we consider line-emission from discrete external BLR-like clouds well outside the central photosphere and tidal radius. In an approach that is initially similar to Gaskell & Rojas Lobos (2014), we focus on a variety of more modern SED models: an AGN spectrum with a spectral slope 1.2 (Baskin, Laor & Stern 2014); and another AGN case with 2.0 (these correspond to the *observed* range of slopes); a blackbody peaking at 4 Ryd; another at 10^6K ; and a hotter 10^7K blackbody (harder than the observed continuum). For comparison with the previous works we also run models using the MF1987 SED.

For each SED, we run several cubes of calculations: exploring a rectangle of $(n_{\text{H}}, \Phi_{\text{H}})$ in steps of 0.1 dex, and saving depth profiles along the N_{H} or spatial axis. We generate cubes where the maximum column was set to $N_{\text{H}} = 10^{23}, 10^{24}, 10^{25} \text{cm}^{-2}$, and then another cube of results where N_{H} was adjusted for each $(n_{\text{H}}, \Phi_{\text{H}})$ so that electron scattering was almost optically thick ($\tau_{\text{es}} = 0.5$). CLOUDY’s approximate representation of scattering becomes less accurate at greater optical depths. We refer the interested reader to Appendix C for the technical details.

Using these calculations, we densely map the range of possible values of H α to He II emission line ratio and He II equivalent widths obtainable when the luminous nuclear source is emitting steadily with a specified SED. Composition is solar. We record intensities from the cloud’s illuminated face, as well as the total including the shadowed face too. These computational surveys proceed in full generality, but we apply the results later (in post-processing) in the contexts of specific astronomical events. Table 1 presents the maximum attainable He II/H α line ratio (w_{\dagger}) from the illuminated side, for each SED model, the cloud parameters where this occurs, and the equivalent widths of five emission lines in these conditions (assuming covering factor, $\Omega = 1$).

Fig. 1 shows the distribution of CLOUDY results for radiation from the illuminated cloud face when $\tau_{\text{es}} \leq 0.5$, in regions of parameter-space near the peak He II/H α . A dot represents every result pair $(I_{4686}/I_{6563}, W_{4686})$ obtained from each input condition $(N_{\text{H}}, n_{\text{H}}, \Phi_{\text{H}})$ in the photoionization parameter cube. Numerically, setting aside precautions against Compton-thick conditions, higher N_{H} enables slightly higher w_{\dagger} , with much the same range of equivalent widths (which is unsurprising because the bright side of an opaque body should dominate radiation from the shadowy parts). For the sake of illustration, we assume a covering factor $\Omega = 0.1$, but the results for another chosen Ω are easily obtained by moving the points appropriately (e.g left, if Ω is reduced). For a specific application, the observation of PS1-10jh is overplotted in cyan, where, using the results and plots of Gezari et al. (2015), the He II line luminosity is $L_{4686} = (9 \pm 1) \times 10^{40} \text{erg s}^{-1}$; the blackbody flux of the observed continuum under the line was $F_{\text{o}} \approx (1.7 \pm 0.3) \times 10^{-17} \text{erg cm}^{-2} \text{s}^{-1} \text{\AA}^{-1}$. The fitted temperature ($T_{\text{o}} \approx 3 \times 10^4 \text{K}$) implies a photospheric luminosity $L_{\text{o}} \approx 8.7 \times 10^{43} \text{erg s}^{-1}$. The He II line’s equivalent width is $W_{4686} = 66.4 \pm 13.9\text{\AA}$. The set of solutions that would be consistent with observations for smaller covering factors ($\Omega < 0.1$ a free parameter) are plotted in black. Grey dots cannot fit PS1-10jh. Orange dots are unphysical cases that would hide *inside* the source (if it were approximately a spherical, opaque *photosphere* surface).

AGN-like spectra (top row of the Figure) produce line ratios compatible with PS1-10jh under a wide range of conditions, however, the He II equivalent widths are *inconsistent* with *any* AGN-like models, even for covering factor much larger than would be realistically expected. (MF1987 might work in unrealistic extreme cloud models, with numerically unsafe $\tau_{\text{es}} > 0.5$, positions within 3 light days of the source, and huge covering factors, $\Omega \gtrsim 0.8$ at 67% confidence.)

Given the failure of these AGN models, we now consider other types of sources, in order to overcome the EW problem. In particular, we consider a set of simple blackbody SED models. For the 4Ryd, 10^6K and 10^7K blackbody mod-

els (bottom row of the Figure) there is an extensive range of plausible solutions that satisfy observational constraints on *both* the line ratio and EW, either for the standard covering factor and even for smaller values ($\Omega \leq 0.1$). The potential disadvantage of these hot sources is that they would be difficult to reconcile with the observed $T_o \approx 3 \times 10^4$ K continuum (which remains steady at late times). Nevertheless, in the following, we suggest a generic scenario which can accommodate these constraints when the luminous source has a varying SED and a light echo occurs.

2.2 A novel scenario: Light-echo photoionization of nuclear clouds

A hard ionizing continuum that peaks at $h\nu \sim 4$ Ryd and a high density gas $n_H \sim 10^{12} \text{ cm}^{-3}$ is required to produce both a strong He II $\lambda 4686$ emission-line and a large He II/H α line ratio. Such densities are observed to occur in the circumnuclear media of AGN (e.g. Netzer 2013). The hard continuum induces high gas temperatures, which makes the He⁺⁺ recombination coefficient larger relative to H⁺; and the high gas density makes the gas optically thick to H α (see Strubbe & Murray 2015). However, observations in the optical of He II-bright TDE candidates are consistent with a black-body continuum source with a temperature T_{BB} of a few 10^4 K only (e.g. Gezari et al. 2012). Two scenarios can alleviate this discrepancy. In the first scenario, two continuum sources exist concurrently: a ‘cold’ source which is observed in the optical; and another ‘hot’ source (e.g. a black body with $kT_{\text{BB}} \sim 4$ Ryd) which ionizes the line-emitting gas. As the ‘hot’ source cools, the ionizing continuum becomes softer, and the object transforms from a He II- to H α -bright. In the second scenario, there is a single continuum source only. The source cools from a very high T (e.g. $T_{\text{BB}} \sim 10^9$ K) to the observed $T_{\text{BB}} \sim 10^4$ K. During a later phase, the source temperature might settle at this level or vary slowly, according to observations. The line-emitting gas resides at a distance of the order of several to a few tens of light-days from the continuum source and from our line-of-sight to the source. The observed line emission is delayed w.r.t. the observed continuum emission. Thus, in He II-bright objects, we measure line emission which corresponds to a continuum source with $kT_{\text{BB}} \sim 4$ Ryd (or more), when the observed continuum source itself has already cooled to $T_{\text{BB}} \sim 10^4$ K. The fading system transforms from He II-bright to He II+H α , and then to H α -bright when the delayed line emission corresponds to an ionizing continuum with $T_{\text{BB}} \lesssim 10^5$ K. This light-echo scenario has a few consequential implications, which are described below.

To observe the ionizing source during its brief, hot, initial phase, TDE candidates must be found in X-rays *before* they are optically detectible. By the time an emission-line light echo appears, the central source has already cooled to $T_{\text{BB}} \sim 3 \times 10^4$ K. Hotter source conditions were briefer and earlier. From this view, it is unremarkable that many UV/O-selected candidates lack X-ray detections (e.g. limits in Table S3 of van Velzen et al. 2016a). A few candidates do possess a relatively constant X-ray counterpart (Holoien et al. 2016a,b). These X-rays may be produced by a corona, by a jet, by reprocessing, or by shocked ISM gas. Our models omit this minor X-ray component, as its contribution to the flux of ionizing photons is negligible.

2.2.1 The continuum source

The continuum during the broad line phases of the UV/O candidates indicates temperatures of $10^4 \text{ K} \lesssim T \lesssim 10^5 \text{ K}$. In time-independent modeling, a luminous source at such temperatures seems unable to photoionize clouds to produce He II and H α equivalent widths in the observed range. Hotter sources could induce emission lines with the observed equivalent widths, but require covering factors orders of magnitude smaller. The lax constraints on Ω are favourable, but the high-temperature continuum is inconsistent with observation. This leads us to the possibility of a time-dependent source, which might provide the best features of both the low- and high-temperature SEDs.

Firstly suppose that the source was a sudden energetic detonation in a (possibly inhomogenous) gaseous medium, at a super-Eddington rate. It might have been a tidal disruption event, a large-amplitude AGN flare, a peculiar kind of superluminous supernova, or any unrecognised new class of explosion with sufficient energy and brevity. Regardless of what the specific injection mechanism might have been, the affected gas will expand as an opaque, radiation-dominated wind or blast-wave. If the injection was abrupt, then the photosphere expands adiabatically with a temperature vs radius relation of $T \propto 1/R$. If there was continuous energy injection, due to the power of a hidden accreting source, then different relations govern the observable light curve.

Next, in order to set spatial and temporal scales, suppose that the hot initial ‘flash’ phase lasted less than a few days. The opaque photosphere, dominated internally by radiation pressure, expands and cools. As the initial flash of hard radiation propagates outwards, it photoionizes circumnuclear clouds or dense debris (perhaps within several light-days of the center). Depending on distance and the evolving luminosity, some clouds emit lines in a He-overbright state, including the strong-EW mode in our 10^7 K calculations. Light from the photosphere reaches telescopes at Earth directly, but line emission from the clouds is delayed by the light-travel time to the cloud (R_c/c , where c is the speed of light). Thus the He-overbright clouds’ emission is superimposed as a light-echo on a later, expanded and cooled view of the nucleus photosphere. Obtaining the observed equivalent widths ($W \sim 60 \text{ \AA}$) and underlying continuum temperature (10^4 K to 10^5 K) implies constraints on the photospheric temperature and luminosity evolution, the covering factor and location of the cloud. The total mass of clouds is derivable from the column density (N_H) assumed in each photoionization model.

In the light-echo model, we suppose that the continuum source is an optically thick photosphere of the flare or wind expanding according to power-laws in time:

$$T \propto t^a \quad (2)$$

$$L \propto t^b \propto T^{b/a} \quad (3)$$

For a blackbody emitting photosphere, the radius

$$R \propto T^x \quad (4)$$

has index $x = [(b/a) - 4]/2$. For an explosion expanding adiabatically at constant velocity, $a = -1$ and $b = -2$. For a relativistic event driven by a power source ($P \propto t^q$), we might have $a = (q - 2)/4(q +$

Table 1. CLOUDY model conditions for a given source SED that give the peak ratio of He II(4686Å) to Hα(6563Å) emission line intensities ($w_{\dagger} \equiv I_{4686}/I_{6563}$) from the illuminated face of the cloud (and limited to cases with low electron scattering optical depths $\tau_{\text{es}} < 0.5$). At the peak, the hydrogen column density, number density, and ionising flux are labelled ($N_{\text{H}}, n_{\text{h}}, \Phi_{\text{H}} = (N_{\dagger}, n_{\dagger}, \Phi_{\dagger})$). The last five columns give the equivalent widths of emission lines, calculated for full coverage ($\Omega=1$) (W_{λ}) for He II, Hα, Hβ, Hγ, Mg II and C IV emission lines (and ‘—’ denotes an absent line). By rows, the illuminating SED was Mathews & Ferland (1987); AGN with slope 1.2; AGN with slope 2.0; 4Ryd blackbody; 10^6K blackbody; 10^7K blackbody.

SED	$\log \bar{\epsilon}$	$\log N_{\dagger}$	$\log n_{\dagger}$	$\log \Phi_{\dagger}$	w_{\dagger}	$\log W_{4686}$	$\log W_{6563}$	$\log W_{4861}$	$\log W_{4340}$	$\log W_{2798}$	$\log W_{1549}$
	(eV)	(cm^{-2})	(cm^{-3})	($\text{cm}^{-2} \text{s}^{-1}$)		(Å)	(Å)	(Å)	(Å)	(Å)	(Å)
MF1987	1.881	23.8	11.7	22.7	5.82	1.08	0.456	0.127	0.0221	-0.0742	1.46
AGN1.2	2.118	23.8	11.8	22.7	4.26	0.732	0.306	-0.0175	-0.164	-0.403	1.20
AGN2.0	2.065	23.8	11.3	22.5	3.62	0.473	0.116	-0.151	-0.268	-0.444	0.962
4Ryd	1.572	23.8	12.0	23.0	6.21	2.79	2.56	1.81	1.52	0.957	1.51
10^6K	2.369	23.5	13.0	25.2	7.90	2.89	2.56	1.95	1.71	—	-7.13
10^7K	3.367	23.4	13.6	24.9	5.96	5.28	5.02	4.28	3.90	—	-2.20

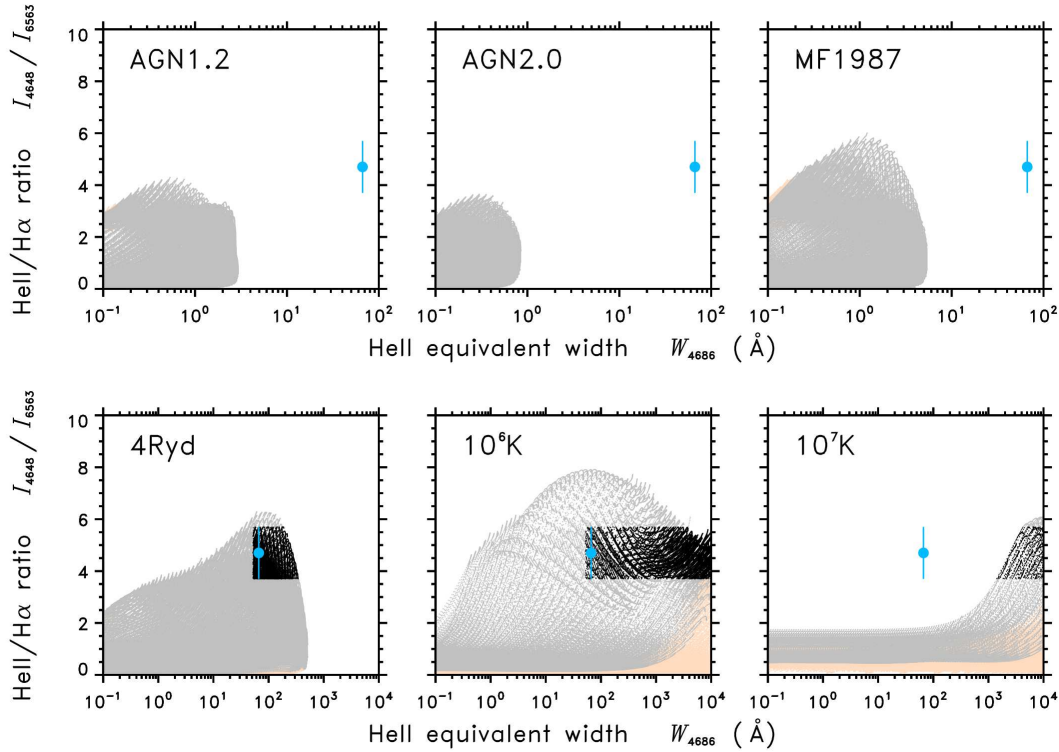


Figure 1. The distribution of possibilities for the I_{4686}/I_{6563} line ratio vs He II equivalent width, assuming a nominal covering factor $\Omega = 0.1$. The top panels assume an AGN-like source; the bottom panels assume a steady blackbody source. The cyan datum shows the observed line ratio and He II equivalent width for PS1–10jh. Black areas are compatible with observations, for the fiducial Ω or smaller. Grey areas fail to match. Orange areas are physically rejected since they would reside inside the photosphere. The source luminosity is assumed to be time-independent, and was normalized to match the observed continuum around wavelength 4686Å. Note that a smaller choice of Ω corresponds to a proportional translation of dots leftwards parallel to the horizontal axis.

2), $b = (2 + 3q)/(2 + q)$ (Blandford & McKee 1976; Cohen & Piran 1999). For some models of the rising phase of a TDE, the indices $a = -7/36$, $b = 11/9$ (Strubbe & Quataert 2009; Lodato, King & Pringle 2009). In the recent Metzger & Stone (2016) model of a TDE’s accretion-powered massive outflow, the temperature initially declines over tens of days, with indices $a = -11/12$ and $b = -5/3$, which approximates adiabatic behaviour well enough. After ~ 30 days of the dimming and cooling, their model’s photospheric temperature steadies (or rises slowly) consistently with late-time T_{BB} in observed UV/O flares. Our calculations omit this stage, because we’re mostly interested in the photoionization echo of the initial flash. The simpler adiabatic model suffices for now.

2.2.2 The line emitting source

We explore a broad realm of possibilities across the $(N_{\text{H}}, n_{\text{H}}, \Phi_{\text{H}})$ space, while correcting the model continuum for the time-lagged expansion of the photosphere. The He II-overbright state is a limited occurrence (e.g. Fig. C1 in Appendix C). It occurs throughout a sausage of the parameter cube, spanning a considerable range in Φ_{H} , implying that He II-brightness can continue a while as the flare fades. Cloud density may be more constraining. Here however, we illustrate the instantaneous possibilities in terms of predicted observables. Fig. 2 shows the He II/H α ratio vs He II, in a light-echo model with PS1-10jh parameters, and assuming a constant-velocity adiabatic expansion of the central source. Black dots are compatible with observations, for our fiducial covering factor or a smaller value ($\Omega \leq 0.1$). In addition to rejecting models where the cloud would reside underneath the photosphere, we also omit cases where R_{c} would exceed 60 light days, as this would be beyond the characteristic scale implied by the 22 day rise time of the observed light-curve. The light-echo model reduces the equivalent widths for the hotter blackbody SED scenarios. When the covering factor is a free parameter, there are still many acceptable fits that have small Ω . The limits from PS1-10jh would require $\Omega > 0.053$ for the 4Ryd model; $\Omega > 6.9 \times 10^{-4}$ for 10^6 K; and $\Omega > 5.5 \times 10^{-5}$ for 10^7 K.

Some observed TDE candidates changed from He II- or H α -bright states to the intermediate case with both He II and H α (Appendix A). None has yet been caught transitioning fully from He II to H α (or vice versa). Theoretically, we do not expect *every* TDE to reach the He II-bright condition, since it occurs in only part of the $(N_{\text{H}}, n_{\text{H}}, \Phi_{\text{H}})$ space: the location and gas density prerequisites are non-trivial (see Fig. C1 in the appendices). Beyond this zone, most flares would begin as H α -bright and end as H α -bright (or lose their broad lines). Catching a complete transformation requires a monitoring campaign with ~ 1 day cadence, spanning many weeks. It is also possible that a seemingly intermediate He II+H α state occurs through superposition, when there are clouds at different locations and densities, which can be He II-bright or H α -bright individually. (ASASSN-14ae’s change from H α -bright to intermediate state might be such a case.)

The emission line broadening results from gas motions. Strubbe & Murray (2015) pointed out that a velocity gradient which is parallel to the radiation reduces the gas opacity. Transparency increases the H α output, and thus reduces the

He II/H α line ratio. We carried out photoionization calculations with ‘turbulent’ velocity which corresponds to the observed line width in PS1-10jh ($\sigma_{\text{turb}} = 5400 \text{ km s}^{-1}$). These calculations indeed result in He II/H $\alpha < 1$. Subsection 3.2 continues to discuss the velocity-opacity problem that could suppress the He II-overbright state.

Fig. 3 shows the predicted luminosities of Mg II emission lines from the illuminated face of the cloud in comparison to the He II luminosity. (in the echo model fiducially assuming $\Omega = 0.1$). The selection of credible solutions for PS1-10jh (marked black) relies only on the H α and He II emission properties, as in Fig. 2. Among the set of solutions that are compatible with PS1-10jh, the Mg II luminosities and can in some cases be comparable to the He II value (up to a few times brighter), but other times undetectable. Under the same model selections, C IV luminosities are distributed similarly: undetectable in many cases, but sometimes exceeding the He II luminosity (by up to ~ 1 dex).

Fig. 4 plots the distribution of cloud mass and position $(M_{\text{c}}, R_{\text{c}})$ for the realistic light-echo model fits to PS1-10jh. Each dot corresponds to one of the successful solutions that were marked black in Fig. 2. Now the colour scale indicates Ω (as a fitted parameter). Many likely locations are at light-days or tens of light-days from the source, which agrees with the light-echo expectations. A few He II-bright solutions exist for clouds located at $\gtrsim 10^2$ light days out. The three rows of this Figure show different constraints on the photoionization models. The top row includes the total line emission from both faces of the cloud, and considers any column density up to $N_{\text{H}} = 10^{25} \text{ cm}^{-2}$. The middle row shows the total line emission, but we omit the opaque clouds with $\tau_{\text{es}} > 0.5$, (where CLOUDY’s approximate treatment of scattering is less realistic). This excludes the higher- M_{c} solutions. In the bottom row, we show only the radiation from the illuminated face of the cloud, which best describes the light-echo scenario. Some of the lowest- M_{c} solutions vanish when the source spectrum is 4Ryd; but the limits for 10^6 K and 10^7 K SEDs aren’t changed significantly. In all cases investigated, we find the following:

- The median cloud masses are subsolar. Taken without bias across the whole parameter space, the masses tend to be planetary in scale. Masses as high as $\sim 0.1 m_{\odot}$ are possible, but require fine-tuning.
- Cloud positions at ~ 10 light days occur naturally, without premeditation or fine-tuning. The implied covering factors are mostly moderate ($10^{-3} \leq \Omega \leq 10^{-1}$), which retrospectively justifies our fiducial assumptions, and supports the light echo scenario.
- At the favoured cloud locations of ~ 10 light days, the orbital velocities would be low enough to solve the velocity problem of the UV/O optical candidates (e.g. discussed by Arcavi et al. 2014). The emission line widths are unrelated to the inner nucleus where the tidal disruption or luminous flare occurs (see Appendix B). They may simply characterize the motions of pre-existing clouds in the impoverished BLR of a previously dormant, declining or erratic weak AGN.

Interestingly, several recent papers have reported infrared light-echo effects from dusty media around TDE candidates. Jiang et al. (2016) and van Velzen et al. (2016b) infer clouds at $\sim 0.1 \text{ pc}$ from the nucleus. Dou et al. (2016) find IR light echo effects over longer timescales, implying more

clouds a few light years farther out. Since circumnuclear material was present over this range of radii, it is not unlikely that there is also gas at even smaller scales, i.e. a few 10 ld (consistent with clouds in our echo photoionization models). These inner clouds would be IR-invisible due to sublimation of their entrained dust. The apparent persistence of some broad emission lines for $\gtrsim 10^2$ days (e.g. ASASSN-14ae [Holoien et al. 2014](#)) might also be an echo effect, in reflections off dust at large distances, and this echo could be prolonged by the convex spatial distribution of reflectors (as in [Dou et al. 2017](#)). The 9000 km s⁻¹ widths of these later delayed emission lines exceeds keplerian velocities of the 0.1 pc zone, but might be the echo of conditions near ~ 10 ld.

3 DISCUSSION

As we discussed above, any acceptable explanation for UV/O TDE-candidates should be able to accommodate both the observed line ratio *and* the EW constraints. Previously suggested, steadily illuminated AGN-like models struggle with this test. [Roth et al. \(2016\)](#) propose an internal, radiative transfer model in which plausible line emission can in some cases emerge from the luminous object's own photospheric structure. We reassert a modified external model, in which the line emission comes from the photoionization light-echo affecting remote BLR-like clouds, tens of light days away. Independent of the origin of the TDE candidates, our echo scenario could reproduce the observations, for various assumed types of transients. Nevertheless, it can constrain details of the explosive origin (within a given theory). In the following subsections, we first discuss direct implications of the light-echo, then overview some of the difficulties with the TDE scenario for the observed UV/O candidates. We consider possible alternatives to TDE origins, including nuclear SNe or intermittency in subluminous/starved AGNs.

3.1 Implications of the light-echo model

3.1.1 Implications for the continuum source

To check several key qualitative properties of the system (to order of magnitude) let us assume a single continuum source that cools from $T_{\text{BB}} \sim 10^9$ to 10^4 K and photoionizes a distant, physically passive gas cloud. We make two additional simplifying assumptions. Firstly, the continuum source is a spherical black body, which cools through adiabatic radial expansion with an adiabatic index of $\gamma = 4/3$ (i.e. dominated by radiation pressure). Secondly, all relevant time scales are of the order of the light travel time from the continuum source to the line emitting gas, i.e. $\tau_c \sim R_c/c$, where R_c is the distance between the source and the cloud, and c is the speed of light. The first approximation is a rough one, as gas with $T \leq 10^6$ K can cool through line emission, which breaks the adiabatic approximation and slows the expansion.

The flux of H-ionizing photons ($h\nu \geq 1$ Ryd) emitted by a black-body with a temperature T_{BB} is approximately

$$\Phi \simeq \frac{4\pi k^3 T_{\text{BB}}^3}{h^3 c^2} \zeta(3) = 1.5 \times 10^{29} T_{\text{BB},6}^3 \text{ cm}^{-2} \text{ s}^{-1}, \quad (5)$$

where k is the Boltzmann constant, h is Planck's constant, ζ is the Riemann zeta function [$\zeta(3) \simeq 1.2$] and $T_{\text{BB}} = 10^6 T_6$ K.² The expression is correct within 2% and 30% for $T_6 \geq 0.5$ and 0.1, respectively. There exists an optimal source T_{BB} (T_{opt}) and corresponding optimal Φ at the illuminated face of the distant cloud (Φ_{opt}) which produce maximal He II and minimal H α emission. These two parameters are somewhat degenerate and depend on the gas column. Good fiducial values are $T_{\text{opt}} \sim 10^6$ K and $\Phi_{\text{opt}} \sim 10^{23} \text{ cm}^{-2} \text{ s}^{-1}$. The radius of a black body with $T = T_{\text{opt}}$ that provides Φ_{opt} at $r = R_c$ is

$$R_{\text{opt}} \approx \sqrt{\frac{\Phi_{\text{opt}}}{\Phi}} R_c = 2.1 \times 10^{13} T_{\text{opt},6}^{-1.5} \Phi_{23}^{0.5} r_{10\text{ld}} \text{ cm}, \quad (6)$$

where $\Phi_{\text{opt}} = 10^{23} \Phi_{23} \text{ cm}^{-2} \text{ s}^{-1}$ and $R_c = 10 r_{10\text{ld}} \text{ ld} = 2.6 \times 10^{16} r_{10\text{ld}} \text{ cm}$ (compatible with the observable time-scale of spectral variations; [Gezari et al. 2012](#); [Holoien et al. 2016b](#)). The assumption of adiabatic expansion implies the continuum source's initial radius,

$$R_i = \left(\frac{T_{\text{opt}}}{T_i} \right)^{4/3\gamma} = 2.1 \times 10^{10} T_{\text{opt},6}^{-0.5} T_{i,9}^{-1} \Phi_{23}^{0.5} r_{10\text{ld}} \text{ cm}, \quad (7)$$

where $T_i = 10^9 T_{i,9}$ K is the initial temperature. This value of R_i is smaller than the expected [Schwarzschild \(1916\)](#) radius ($R_\bullet \sim 10^{12} \text{ cm}$ for $m_\bullet = 10^7 m_\odot$). However, the continuum source in our model is not limited to a TDE (see above, and later in subsections 3.3.1, 3.3.2). For stellar explosions in the parsec-scale nuclear star cluster, R_\bullet is inapplicable. In an AGN jet context, it is conceivable for transient luminous features to vary on scales smaller than R_\bullet (e.g. [Aleksić et al. 2014](#)). Thus $R_i > R_\bullet$ is not required. It should be noted that if $T_i \sim 10^6$ K, rather than 10^9 K, then $R_i \sim R_\bullet$ and is consistent with a TDE origin of the continuum source (see also below). Mutatis mutandis, the adiabatic phase ends at a final radius

$$R_f \sim 2.1 \times 10^{14} T_{\text{opt},6}^{-0.5} T_{f,5}^{-1} \Phi_{23}^{0.5} r_{10\text{ld}} \text{ cm}, \quad (8)$$

where $T_f = 10^5 T_{f,5}$ K. We use $T_f \sim 10^5$ K rather than 10^4 K, since below $T \sim 10^5$ K radiative cooling dominates and expansion slows significantly. Until then, the photospheric expansion velocity is approximately

$$v_{\text{exp}} \sim \frac{R_f}{R_c/c} = 2400 T_{\text{opt},6}^{-0.5} T_{f,5}^{-1} \Phi_{23}^{0.5} \text{ km s}^{-1}. \quad (9)$$

Note that v_{exp} is independent of the assumed R_c . The He II-bright state is produced from $T_{\text{BB}} = 10^6$ K down to 10^5 K, i.e. 1 dex in T_{BB} . Since $T_{\text{BB}} \propto R^{-1}$ (eq. 7), the cloud remains in the He II-bright state for a time of at least

$$\Delta t \approx 10 R_{\text{opt}}/v_{\text{exp}} = 10 T_{\text{opt},6}^{-1} T_{f,5} r_{10\text{ld}} \text{ d}, \quad (10)$$

where we used eq. (6). The *apparent* broad-line phase could be prolonged by contributions from multiple clouds in different orbits, or monochromatic reflections off distant dust. By eq. (10), the hard X-ray beginning was brief enough ($\lesssim 0.1$ day) to go undetected before the UV/O transient became conspicuous.

² Although the discussion focuses on line emission of He II which requires photons with $h\nu \geq 4$ Ryd, we include photons already from $h\nu \geq 1$ Ryd in Φ , as this is the standard definition of Φ in photoionization codes (e.g. CLOUDY).

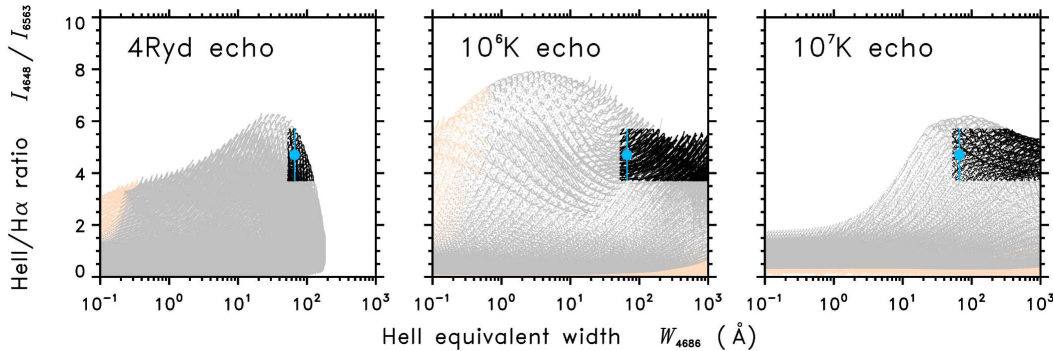


Figure 2. The distribution of line ratios vs He II equivalent widths in with continuum evolution in blackbody light-echo models. The assumed photosphere expands adiabatically at constant velocity, illuminating a cloud with covering factor $\Omega = 0.1$. As in Fig. 1, black dots are solutions consistent with observations (when $\Omega \leq 0.1$); the PS1–10jh data are the cyan dot; unphysical solutions are orange; observationally incompatible points are grey.

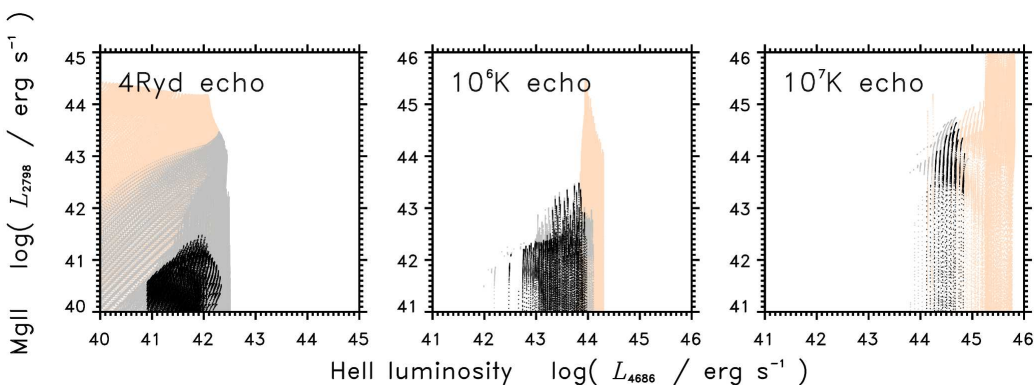


Figure 3. The distributions of predicted Mg II line luminosity (vertical axes) vs He II (horizontal axes) from blackbody light-echo models. Solutions are selectively coloured (as in Fig.1) for their consistency with H α and He II observed from PS1–10jh.

Assuming isentropic expansion and using eq. (9) we can infer the total mass M of the continuum source. The velocity of isentropic expansion is approximately

$$v_{\text{ise}} \approx \frac{2}{\gamma - 1} \sqrt{\gamma \frac{aT_i^4/3}{M(4\pi R_i^3/3)^{-1}}}, \quad (11)$$

where $a = 4\sigma/c$, and σ is the Stefan-Boltzmann constant (e.g. Zel'dovich & Raizer 1967). Taking $v_{\text{ise}} = v_{\text{exp}}$ and inserting eq. (7) yields $M \approx 4 \times 10^4 T_{i,9}^{-0.5} T_{\text{opt},6}^2 T_{5,f}^2 \Phi_{23}^{0.5} r_{10\text{ld}}^3 m_{\odot}$. The total bolometric luminosity across the photosphere is

$$\begin{aligned} L_{\text{bol}} &= 4\pi R^2 \sigma T_{\text{BB}}^4 = 4\pi R_{\text{opt}}^2 \sigma T_{\text{opt}}^2 T_{\text{BB}}^2 \\ &= 3.2 \times 10^{45} T_5^2 T_{\text{opt},6}^{-1} \Phi_{23}^2 r_{10\text{ld}}^2 \text{ erg s}^{-1}, \end{aligned} \quad (12)$$

where $T_{\text{BB}} = 10^5 T_5$ K. This estimated L_{bol} is broadly consistent with observations (van Velzen et al. 2011; Cenko et al. 2012a; Chornock et al. 2014; Cenko et al. 2016; Holoien et al. 2016b). Thus, an adiabatic expansion predicts that for $v_{\text{exp}} t \gg R_{\text{in}}$, $L_{\text{bol}} \propto t^{-2}$. The total energy emitted during the adiabatic-expansion phase is

$$\begin{aligned} E &\sim \int_0^{R_c/c} L_{\text{bol}} dt \simeq \frac{4\pi\sigma R_{\text{opt}}^4 T_{\text{opt}}^4 R_c}{R_i R_f c} \\ &= 3 \times 10^{55} T_{\text{opt},6}^{-1} T_{i,9} T_{f,5} \Phi_{23}^3 r_{10\text{ld}}^3 \text{ erg}. \end{aligned} \quad (13)$$

This energy scale (13) and the mass derived from equation (11) imply some interesting parameter constraints, de-

pending on what type of explosive event erupted into the continuum source. Taking fiducial input values, the estimate (13) exceeds the energies of super-luminous SNe by a factor of $\sim 10^3$ (Gal-Yam 2012; Inserra et al. 2013; Vreeswijk et al. 2014; Dong et al. 2016). The corresponding mass $M \sim 2 \times 10^4 m_{\odot}$ would also be extraordinary for a stellar progenitor. The energy implied by eq. (13) would also require extraordinary mass accretion or annihilation ($E/\eta c^2$, with $\eta < 0.1$) besides inefficiencies such as neutrino production, and would exceed the observational fluence estimates. What are the alternatives? More detailed tests show that the energy and progenitor mass are sensitive to details of different γ and models of the photosphere's expansion. A softer equation of state with $\gamma = 5/4$ yields $M \sim 10 m_{\odot}$ (and a corresponding $R_i \sim 10^9$ cm). The smaller value of γ is relevant for the highest T and small R , where the source conditions may be favourable for pair production, reducing γ below $\gamma = 4/3$. (Plausibly, some entrainment of upswept circumnuclear gas might also alter γ .) Alternatively, a lower initial temperature ($T_{i,9}$) could be an explanation. Replacing R_i with R_{opt} in eq. (13) (i.e., starting the integration at $T_{\text{BB}} = 10^6$ K rather than 10^9 K) yields $E \sim 3 \times 10^{52}$ erg, consistent with observations, and more compatible with a stellar event such as a supernova (subsection 3.3.1). Thus the continuum source energy problem is both flexible and

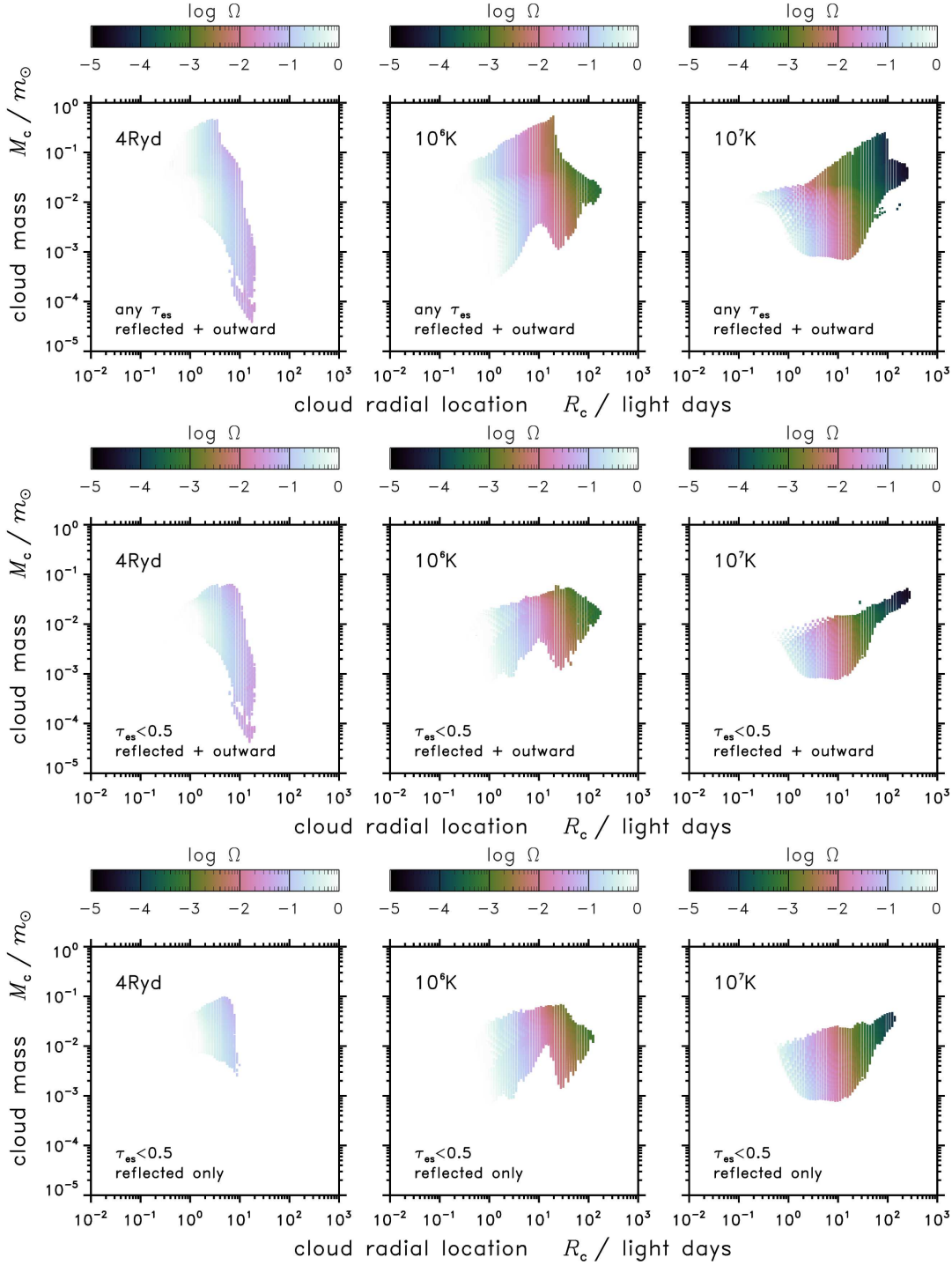


Figure 4. Distributions of possible cloud masses (M_c) and locations (R_c) that are compatible with PS1–10jh observations, for some covering factor (Ω , now a fitted parameter). Columns show three blackbody light-echo models. Colours indicate the cloud covering factor. Only the observationally consistent solutions (black in Fig. 1) are shown. The implied cloud mass never exceeds a subsolar value.

sensitive to subtle details of the flare’s expansion and cooling evolution (at this back-of-the-envelope level). The properties of the external photoionized cloud are more robustly constrained, and we discuss those firmer findings next.

3.1.2 Implications for the line-emitting gas

To produce a He II-bright state, the line-emitting gas must react to variations in the ionizing continuum quicker than the variability time-scale of the continuum source. Two time-scales affect the gas: the ionization and recombination time-scales. The gas reacts to changes in the continuum the longer of these two scales. We continue to use $\tau_{\text{var}} \equiv R_c/c =$

$8.6 \times 10^5 r_{10\text{ld}}$ s as the variability time-scale of the continuum. The ionization time-scale τ_{ion} can be estimated as follows. The photoionization cross-section of He^+ that is averaged over a black-body continuum ($\bar{\sigma}$) is approximately

$$\bar{\sigma} \approx \begin{cases} 1.41 \times 10^{-18} T_6 \text{ cm}^2, & \text{for } 0.1 \leq T_6 < 0.3 \\ 1.10 \times 10^{-19} T_6^{-1.7} \text{ cm}^2, & \text{for } T_6 \geq 0.3 \end{cases}, \quad (14)$$

where we use the expression for $\sigma(\nu)$ from [Verner & Ferland \(1996\)](#). The approximation is correct within a factor of 3. The implied $\tau_{\text{ion}} \equiv 1/\bar{\sigma}\Phi$ is

$$\tau_{\text{ion}} \approx \begin{cases} 7 \times 10^{-6} \Phi_{23}^{-1} T_6^{-1} \text{ s}, & \text{for } 0.1 \leq T_6 < 0.3 \\ 9 \times 10^{-5} \Phi_{23}^{-1} T_6^{1.7} \text{ s}, & \text{for } T_6 \geq 0.3 \end{cases}. \quad (15)$$

Thus, $\tau_{\text{ion}} \ll 1$ s for $\Phi_{23} \sim 1$ and $T_{\text{opt},6} \sim 1$, and is negligible compared to τ_{var} . The assumption of adiabatic expansion yields $\tau_{\text{ion}} \ll \tau_{\text{var}}$ also for $T_6 \sim 1000$, i.e. when the continuum source is at maximum T_{BB} , since $\Phi_2 = \Phi_1 T_2/T_1$ (eqs. 5 and 7). The constraint on the recombination time scale, $\tau_{\text{rec}} \equiv 1/\alpha n_{\text{gas}} < \tau_{\text{var}}$, implies a lower limit on the gas number density n_{gas} , where α is the recombination coefficient. We approximate the dependence of α of He^{++} on T_{gas} by $\alpha \approx 10^{-7} T_{\text{gas}}^{-1.07} \text{ cm}^3 \text{ s}^{-1}$ ([Verner & Ferland 1996](#)), which is accurate within a factor of 2.5 in the $10^4 \leq T_{\text{gas}} \leq 10^9$ K range. The implied constraint on the gas density is

$$n_{\text{gas}} > \frac{1}{\alpha} \frac{1}{R_c/c} \approx 3 \times 10^6 T_{\text{gas},5}^{1.07} r_{10\text{ld}}^{-1} \text{ cm}^{-3}, \quad (16)$$

where $T_{\text{gas}} = 10^5 T_{\text{gas},5} \text{ K}$.³ This value of n_{gas} is well below $n_{\text{gas}} \sim 10^{12} \text{ cm}^{-3}$ which is required by photoionization calculations to produce the observed high $\text{He II}/\text{H}\alpha$ line ratio.

3.2 Puzzles and difficulties for the TDE model

Several puzzles and problems emerge from observational studies of TDE candidates (see [Komossa 2015](#)), and may suggest that these events might not arise from tidal disruptions by MBHs, but rather from other sources. Here we only focus on issues relating to our results, and later discuss possible alternative origins.

1. In some systems, the inferred mass accretion is subsolar (see also discussion in section 2.2.1), and indeed much less than any likely donor star. For UV/O candidates, the most credible estimates appear subsolar ([Renzini et al. 1995](#); [Gezari et al. 2012](#); [Chornock et al. 2014](#); [Holoien et al. 2014](#)). ASASSN-14ae was discovered after its peak, but the accretion was only $\gtrsim 0.001 m_{\odot}$ ([Holoien et al. 2014](#)). A similar limit from iPTF16axa gives $3.1 \times 10^{-3} m_{\odot}$ ([Hung et al. 2017](#)). More clearly subsolar events include iPTF16fnl with $< 10^{-4} m_{\odot}$ ([Blagorodnova et al. 2017](#)); PS1-11af with $0.002 m_{\odot}$ ([Chornock et al. 2014](#)); ASASSN-14li with $0.004 m_{\odot}$ ([Holoien et al. 2016a](#)); ASASSN-15oi with $0.003 m_{\odot}$ ([Holoien et al. 2016a](#)); PS1-10jh with $0.012 m_{\odot}$ ([Gezari et al. 2012](#)); and $0.004 m_{\odot}$, $0.11 m_{\odot}$ for two transients of [Gezari et al. \(2008\)](#). Allowing host galaxy extinction may be compatible with accretion $\lesssim 0.1 m_{\odot}$ in

³ We use the scaling of $T_{\text{gas}} \sim 10^5$ K in eq. (16), as it is roughly the thermodynamic equilibrium T of gas that is located at a distance R_c from a continuum source with $T_{\text{BB}} = T_i \sim 10^9$ K, i.e. $T_{\text{gas}} \approx T_i \sqrt{R_i/R_c}$ (see eq. 7).

PTF09ge ([van Velzen et al. 2016b](#)) and $0.06 m_{\odot}$ in D23H-1 ([Gezari et al. 2009](#)). Bolometric corrections might explain these two events as stellar TDEs, but the transients with lower accretion estimates are more challenging to explain.

[Guillochon, Manukian & Ramirez-Ruiz \(2014\)](#) matched PS1-10jh chromatic light-curves to simulations of a $4 m_{\odot}$ or $0.5 m_{\odot}$ star in a sub-Eddington TDE plus translucent outflow (but without detailed fitting of line luminosities or EW). If a normal star was only partially disrupted (e.g. [Guillochon & Ramirez-Ruiz 2013](#)) this could explain the transient’s low mass budget, but flaring should eventually recur on timescales comparable to the orbital period of the remnant stellar core. Since no secondary flare has been reported, the partial TDE scenario would require orbital periods longer than several years (in every known TDE candidate). Though earlier models find that half of TDE debris remains bound, [Metzger & Stone \(2016\)](#) argue that a TDE with sufficient Eddington ratio ejects most of the gas into an opaque, radiation dominated outflow; and only a minority accretes. Alternatively, it might be that the accretion process was radiatively inefficient for some unknown reason; perhaps because the tidal stream’s self-intersection shock has been delayed by orbital precession effects or other complications ([Guillochon & Ramirez-Ruiz 2015](#); [Piran et al. 2015](#); [Svirski, Piran & Krolik 2017](#)). Unless one of more of these remedies applies to all UV/O candidates, the observed low mass indicators reveal something unexpected about the accretion source.

2. For the UV/O TDE candidates, the emission line widths tend to be less than the orbital velocities expected at R_t , or else the emission region is radially much larger than expected from stellar disruption ([Gezari et al. 2009, 2012](#); [Arcavi et al. 2014](#); [Chornock et al. 2014](#)). A potential solution could invoke debris circularization occurring far from the tidal-disruption radius, ([Piran et al. 2015](#); [Svirski, Piran & Krolik 2017](#)) but whether this is indeed the culprit is still an open question. [Roth et al. \(2016\)](#) and [Metzger & Stone \(2016\)](#) attribute the line widths to random transverse motions (eddies?) on the central source’s photosphere, as it expands at $\sim 10^4 \text{ km s}^{-1}$. (Detailed hydrodynamic models, including temporal variability, aren’t yet available.) We ran CLOUDY tests of $> 10^3 \text{ km s}^{-1}$ turbulent photoionized slabs, and always find that the kinematically reduced $\text{H}\alpha$ opacity prevents $\text{H}\alpha$ suppression, which prevents the He II -overbright state. An orderly outflow with radial velocity gradients would also suffer the problem of $\text{H}\alpha$ -transparency. We suggest that He II -overbrightness arises more easily from a population of well separated clouds, each with low internal velocities, but high velocity dispersions among them as an *ensemble*. We further discuss the line velocity scaling and present the relevant data in the Appendix B.

3. Reviewing a set of UV/O candidates, [Arcavi et al. \(2014\)](#) noted that most TDE host galaxies seem weak in star formation, and several belong to the rare E+A ‘post-starburst’ type. Exceptionally, [Holoien et al. \(2014\)](#) report a candidate in a spiral galaxy. E+A ‘post-starburst’ galaxies show stellar absorption lines indicating a stellar population truncated at a few Gyr age, and ongoing star formation is weak or regionally limited ([Dressler & Gunn 1983](#); [Yamauchi & Goto 2005](#); [Brown et al. 2009](#); [Pracy et al.](#)

2014). They often exhibit disturbed morphologies or close tidally interacting companion galaxies (Yang et al. 2004; Kewley, Geller & Barton 2006; Goto et al. 2008; Pracy et al. 2009) suggesting the possibility of relatively recent (Gyr) galaxy mergers. If a galaxy nucleus contains a binary SMBH then 3-body scattering will gradually harden their orbit to a pc-scale separation, while ejecting many stars and incurring tidal disruptions more often than a single supermassive object would (e.g. Quinlan 1996; Ivanov, Polnarev & Saha 2005; Chen et al. 2009, 2011; Wegg & Nate Bode 2011). A significantly non-spherical stellar background potential could also increase the TDE rate (e.g. Vasiliev 2014; Hamers & Perets 2017). Since SMBH binaries and asymmetric potentials are both expected outcomes of galaxy mergers, it may be that the overabundance of TDE-candidates in these galaxies is related to their relatively recent galaxy merger history. However, the expected increased TDE rates are typically at most a few times larger, while the inferred flaring rates in these hosts seems at least an order of magnitude (if not more) larger than expected given the rarity of E+A galaxies (only as few as $\lesssim 10^{-2}$ of all galaxies; Zabludoff et al. 1996; Goto et al. 2003; Quintero et al. 2004; Vergani et al. 2010).

Circumnuclear power-law cusps of stellar density should raise TDE rates, in theory (Magorrian & Tremaine 1999; Wang & Merritt 2004). If the apparently steep young cusp of one E+A galaxy (NGC 3156, $\rho_{\star} \propto r^{-2.2}$ at ~ 4 pc resolution) continues to radii $\ll 0.1$ pc, then this might explain the TDE productivity of this class (Stone & Metzger 2016; Stone & van Velzen 2016). It is unknown how long steep stellar cusps survive dynamically, and whether they are special to the E+A phase of galaxy evolution.

Some E+A galaxies seem to feed low-luminosity AGN (Yang et al. 2006), and the evidence of an intermediate (Gyr ago) star-formation epoch suggests the existence of a gas reservoir, which is lower than star-forming galaxies, but can be sufficient for a spasmodic, low rate feeding of an AGN, potentially producing starved/subluminous AGNs. If the TDE-candidate flares are not bona-fide TDEs but are related to bursts from subluminous AGNs (a possibility discussed in the next section), then such E+A galaxies might indeed provide favourable conditions, and explain why such nuclear flares preferentially reside in E+A hosts.

3.3 Alternative (non TDE) origins for TDE-candidates

3.3.1 A supernova among circumnuclear clouds

The nuclear regions of many galaxies may be favourable locations for concentrated episodes of supernova activity. The quiescent Milky Way's inner 0.1pc produced massive stars ~ 1 Myr ago (e.g. Bartko et al. 2010), which will yield a local SN rate of a few 10^{-5} yr^{-1} : within reach of predicted TDE rates. Evidence that the central object Sgr A* fluctuates over ~ 500 yr (e.g. Ryu et al. 2013) also implies a variable gas supply to a starved AGN (some of which might be diverted to star formation). Stronger circumnuclear starbursts in highly disturbed galaxies might conceivably yield enough SN to confuse cosmic TDE monitoring.

While the continuum source of TDE candidates may be explained by a (super-luminous) SN explosion, the re-

quired density of line-emitting gas in He II-bright cases ($n_{\text{gas}} \sim 10^{12} \text{ cm}^{-3}$) is large compared to the densities expected for the ISM of quiescent galaxies. Such a large n_{gas} is however typical in nuclear regions of AGN (e.g. Netzer 2013). French, Arcavi & Zabludoff (2016) report that TDE detections are preferentially found (40%–75%) in Balmer-strong galaxies, i.e. galaxies that recently had a strong starburst (roughly within the last Gyr). These galaxies are only 0.2% of the local galaxy population. A strong starburst requires a large supply of gas, a fraction of which may reach the host nucleus and feed an AGN. This activity quenches star formation in the nuclear region; the only exception is the parsec-scale dusty torus where starbursts may occur continuously throughout the life of AGN (Collin & Zahn 1999a,b; Sirko & Goodman 2003). Thus, a candidate TDE may be the SN explosion of a progenitor star that formed locally within the torus. (This region is circumnuclear but far outside the event horizon and hot inner accretion disc, and therefore not directly related to the horizon size.) The explosion occurs sometime after the AGN falls dormant ($\lesssim 10^3$ yr), before the dense clumps of gas disperse (or collapse). An AGN has a life-time of $\sim 10^8$ yr. A star of a few $10m_{\odot}$ lives for a few 10^7 yr. Thus, the expected fraction of TDE candidates in quiescent Balmer-strong galaxies is $\sim 10^7/10^8 = 10\%$, consistent with observations (French, Arcavi & Zabludoff 2016). SN explosions occurring after the nucleus has lost its denser clumps miss the He II-bright phase. This scenario naturally explains the observed emission-line width of a few 1000 km s^{-1} which is typical of the BLR region of AGN.

The SN-explosion scenario for TDE imposters may also explain the peculiar SNe of type II-L and II-P, which exhibit spectral behaviour similar to He II-bright TDE candidates (Smith et al. 2015). These are likely SN explosions of massive progenitors that detonate near a reservoir of dense gas (e.g. protostellar clouds). A possible connection between TDE candidates and extreme SNe was previously pointed out by others (Komossa et al. 2009; Drake et al. 2011). Here, we establish this connection from photoionization considerations. Gezari et al. (2009) disfavour the connection, pointing out that the UV continuum emission (i.e. $T_{\text{BB}} \gtrsim 10^4 \text{ K}$) fades significantly faster in SNe compared to TDE candidates (weeks versus months). This discrepancy may be explained by the denser ISM than expected in a galactic nucleus. Ambient gas confinement could alter the SN shock physics and radiative efficiency, producing an abnormally shallow light-curve. Finally, we note that similar links between nuclear SNe and AGN activity has been suggested before (e.g. Terlevich et al. 1992; Aretxaga & Terlevich 1994; Ulrich, Maraschi & Urry 1997; Aretxaga 1999).

3.3.2 Subluminous AGN flaring scenario

Another alternative possibility is that the UV/O TDE candidates could have been a type of unrecognized flaring from accretion onto a MBH, possibly in a subluminous/starved AGN that lacks strong emission line regions during a long semi-quiescent state. Circumnuclear clouds may be present, but normally not irradiated strongly enough for an observable BLR (or NLR). Some hosts may be senescent or starving AGN, which have already accreted most

of the available interstellar gas. These could be related to AGNs that change their BLR type and/or missing them (e.g. Tran 2001; Bianchi et al. 2005; Zhang & Wang 2006; Kaastra et al. 2014), which can occur even on short timescales (Storchi-Bergmann, Baldwin & Wilson 1993; Aretxaga 1999; Shappee et al. 2014; Oknyansky et al. 2016; McElroy et al. 2016). Some peculiar types of AGNs could play a similar role, e.g. XBONG sources (Elvis et al. 1981; Griffiths et al. 1995; Comastri et al. 2002; Fiore et al. 2003; Severgnini et al. 2003; a few of which are E+A galaxies Kim et al. 2006). In particular, variability in blazars and BL Lac objects can exceed several optical magnitudes (Eggen 1973; Xie et al. 2002; Dolcini et al. 2005; Danforth et al. 2013; Sandrinelli, Covino & Treves 2014).

Indeed, there are a few possible examples. Campana et al. (2015) proposed a reverse argument — explaining recurrent AGN flaring as TDE in the weak AGN in IC 3599. Alloin et al. (1986) observe recurrent outbursts in a low-powered AGN, each of which behaved like an intermediate phenomenon between modern TDE candidates and the normal activity of a steady AGN, while Saxton et al. (2015) suggested to relate a transient TDE-like event to a disc instability around a weak AGN in NGC 3599.

Laor (2003) proposed that shear destroys any BLR clouds within a limiting orbital radius, but the number of clouds irradiated enough to emit the broad lines depends on the nucleus' luminosity. Consequently, an AGN weaker than some threshold will not have any observable BLR. It is therefore conceivable that a nuclear *brightening* in a previously *unrecognised* AGN can activate previously unilluminated BLR clouds, giving the false appearance of a TDE. This depends on the weakness of ordinary AGN signatures in the initial state, and the availability of at least one non-luminous circumnuclear cloud initially outside the Laor (2003) limiting radius. Flaring might be fed by an episodic surge of accretion: a disc instability, an abrupt change in accretion state, or passage of a massive object through the disc. Accretion might increase if a new gas source arrives, derived from a cloud that has scattered into a diving orbit, much like the disruption of a star. Whatever the trigger and the fuel, flaring then excites one or more previously dormant circumnuclear clouds; if they cover enough of the nucleus then the result is a transient BLR. One then still needs to explain the lack of hard radiation from the inner parts of the disc (perhaps due to an inner disc cavity).

Among conceivable flaring processes around MBHs, the disc-instability model of Kim (2010) might be extended from microquasars to instability in a disc around a MBH. In this case, an instability in the inner accretion disc can lead to draining of the inner region, producing a cavity, while the accreted material powers a flare. The flaring can later be echoed by more distant material, (as described in the echo model). Stochastic recurrence timescales might be longer for larger m_{\bullet} , with testable consequences in population statistics (van Velzen 2017). Given the observational selection bias against AGN hosts, such events are likely to be identified only in cases where a gaseous disc exists around a MBH, but the accretion is insufficient to power an observable AGN, e.g. in cases of starved or subluminous AGNs, where circumnuclear gas exist, but is scarce. These might possibly corre-

spond to E+A galaxies, in which star-formation and hence gas supply were abundant in the relatively near (but not recent) past, while the MBH now feeds only on the (now dwindling) gas inflow following the past merger event. Even drier galaxies would not have sufficient supply, and the MBH would not sustain a disc in which instabilities could occur.

Another model by Tanaka (2013) involving binary MBH may also be relevant. The binary clears a central cavity in its accretion disc, which appears dimmer and softer than an equivalent single-AGN disc. Depending on the binary period, intermittent gas streams of perhaps $0.1m_{\odot}$ dive towards the SMBHs from the cavity's lip. Each stream shocks near the recipient SMBH, causing a flare resembling a TDE. If the recurrence period is long compared to the era of transient monitoring, then a single detection could be misidentified as a TDE. The recurrence period, debris velocities and energy yields in a cavity flare depend on the binary separation, and need not correspond to predicted tidal radii of stellar disruptions. Timescales of cavity flares need not show any clear relation to SMBH masses (c.f. van Velzen 2017). Subtler details might distinguish binary cavity flares: the steepness of their fading, or occurrence around a SMBH that is too massive for a TDE. (For example, Leloudas et al. 2016 recently infer $m_{\bullet} > 10^8 m_{\odot}$ in the weak-lined TDE candidate ASASSN-15lh.) If SMBH binaries are a common product of the mergers forming E+A galaxies, then the cavity flare mechanism might explain the peculiar incidence of UV/O nuclear transients in these hosts.

Let us consider generically what happens as the amplitude of an AGN flare is increased (whether it involves jet internal shocks, or an accretion surge from disc instability). For a small-amplitude event, the rising and the fading involve similar physics, and phenomena are almost reversible in time. A more luminous flash exerts an impulsive radiation pressure on opaque circumnuclear clouds. At greater intensities, the peak luminosity exceeds the local Eddington limit, driving a radiation-dominated outflow, which could in turn drive external shocks into the ISM, resulting in a prolonged, fading afterglow like those of gamma-ray bursts. The emergent luminosity is limited to a few times L_E , but a radiation-driven wind could carry more kinetic power. Thus an asymmetry between rising and fading rates is naturally expected for higher-amplitude events.

If the energy injection is abrupt and intense enough to propel an *opaque* radiation-dominated explosion then the responsible process is concealed. In super-Eddington models, the wind photosphere hides the accretion disc and accretor (e.g. Strubbe & Quataert 2009; Metzger & Stone 2016). This explains why late-time UV/O candidate temperatures are a few times 10^4 K, rather than the 10^5 K temperatures expected for matter near the tidal radius (e.g. Jaroszynski, Abramowicz & Paczynski 1980; Loeb & Ulmer 1997; Ulmer 1999). This generic self-concealment of super-Eddington events implies that a high-amplitude AGN outburst may be practically difficult to distinguish from a TDE flare, or an unusual supernova detonating in a dense medium (Smith et al. 2015; Moriya et al. 2017). In this way, the continuum source may be the *least* informative aspect of the transient, and other identifying signatures are needed. Transient radio, X-ray and γ -ray components could be the result of collimated jets erupting through the opaque surface: briefly, persistently, or with instabilities and pre-

cession effects depending on idiosyncrasies of each system (e.g. Gezari et al. 2009; van Velzen, K rding & Falcke 2011; Bloom et al. 2011; Levan et al. 2011; van Velzen et al. 2013; Saxton et al. 2012; Cenko et al. 2012b; Bower et al. 2013; van Velzen et al. 2016a; Alexander et al. 2016). In events where jets ceased after an initial burst, their emissions might ionize distant clouds, like the early hot photosphere’s ‘flash’ in our light-echo models.

4 CONCLUSIONS

In this study we explored the spectral features of tidal disruption event candidates. Our analysis shows that standard AGN-like irradiation models cannot explain both the origin of the line ratios as well as the individual equivalent widths seen in observations. We find that models of blackbody illumination of remote BLR-like clouds ($n_{\text{gas}} \sim 10^{12} \text{ cm}^{-3}$) could yield realistic line emissions across a significant range of conditions, but only when considering a hot source (10^6 K), while a 10^4 K blackbody is consistent with the continuum observed in UV/O TDE candidates. We propose a novel light-echo model to resolve these difficulties, and this has important implications for the early evolution of the explosive event and the later temporal evolution of the spectral features. In the light-echo model, an initial hard radiation flash illuminates BLR clouds residing at distances on the order of ten light-days. Their strong line emission is then seen delayed and superimposed on the softer continuum emitted later from the exploded source. Our model can therefore provide a prediction that TDE candidates should appear X-ray bright in the continuum before the He II state.

This light-echo photoionization modelling is generic to near-super-Eddington outbursts in a galaxy nucleus, as long as there are some BLR-like external clouds at suitable distances. Diffuser clouds only exhibit the H α -bright or fully ionized states. It could be difficult to distinguish between a tidal disruption event, an outburst by an impoverished AGN, or an exotic superluminous supernova, or perhaps other explosive transients not yet recognized. A weak, starving AGN accreting at a low average rate, with a nearly exhausted gas supply, might mimic a TDE if a high-amplitude flare photoionizes the few clouds of a normally dim and impoverished BLR. A superluminous supernova detonating among the dense BLR clouds could have a similarly evolving outflow, hiding the central engine. For each single cloud in any of these types of system, the occurrence of a He II-bright state depends on whether it evolves through a limited sausage-shaped zone of the $(N_{\text{H}}, n_{\text{H}}, \Phi_{\text{H}})$ parameter cube. Densities of $10^{11} < n_{\text{H}} < 10^{13} \text{ cm}^{-3}$ are necessary but not sufficient. Brightening, fading and temperature changes by the central source control Φ_{H} , while $(N_{\text{H}}, n_{\text{H}})$ might change if the cloud derives from ballistically evolving TDE debris (e.g. Guillochon, Manukian & Ramirez-Ruiz 2014). Transitions between He II-bright, He II+H α , and H α -bright states are conceivable. Multiple clouds and reflections off remote dust may complicate the collective spectra. In future, time-dependent emission line models and higher-cadence spectroscopic monitoring will test these possibilities. It would also be valuable to explore intermediate cases between the theory of a line emission hugging an opaque photosphere (Roth et al. 2016, despite the challenge of velocity and H α -

transparency) and our model of light-echo photoionization of distinct BLR clouds (methodologically constrained by $\tau_{\text{es}} < 0.5$). Temporal variability of the spectra, testing the photoionization light echo time-lags, may be essential to discriminating among these models and diagnosing their spatial structures.

ACKNOWLEDGEMENTS

We thank the referee N. Murray for his constructive criticism; and we thank B.D. Metzger, N.C. Stone, S. van Velzen, A. Laor, I. Arcavi and S. Kaspi for helpful discussions. This work has made use of NASA’s Astrophysics Data System. Calculations were performed with version 13.03 of CLOUDY, last described by Ferland et al. (2013). This publication has made use of code written by James R. A. Davenport.⁴ Specifically, the figure color scheme⁵ was developed by Green (2011). CJS and HBP acknowledge support from the Israel Science Foundation through the astrophysics I-CORE program 1829/12. CJS thanks D.M. Greer, R. & R. Whittaker for their hospitality during this work.

REFERENCES

- Aleksi c J. et al., 2014, *Science*, 346, 1080
 Alexander K. D., Berger E., Guillochon J., Zauderer B. A., Williams P. K. G., 2016, *ApJ*, 819, L25
 Alloin D., Pelat D., Phillips M. M., Fosbury R. A. E., Freeman K., 1986, *ApJ*, 308, 23
 Arcavi I. et al., 2014, *ApJ*, 793, 38
 Aretxaga I., 1999, in *IAU Symposium*, Vol. 193, Wolf-Rayet Phenomena in Massive Stars and Starburst Galaxies, van der Hucht K. A., Koenigsberger G., Eenens P. R. J., eds., p. 716
 Aretxaga I., Terlevich R., 1994, *MNRAS*, 269, 462
 Baldwin J., Ferland G., Korista K., Verner D., 1995, *ApJ*, 455, L119
 Bartko H. et al., 2010, *ApJ*, 708, 834
 Baskin A., Laor A., Stern J., 2014, *MNRAS*, 438, 604
 Bianchi S., Guainazzi M., Matt G., Chiaberge M., Iwasawa K., Fiore F., Maiolino R., 2005, *A&A*, 442, 185
 Blagorodnova N. et al., 2017, *ApJ*, 844, 46
 Blandford R. D., McKee C. F., 1976, *Physics of Fluids*, 19, 1130
 Bloom J. S. et al., 2011, *Science*, 333, 203
 Bower G. C., Metzger B. D., Cenko S. B., Silverman J. M., Bloom J. S., 2013, *ApJ*, 763, 84
 Brown M. J. I. et al., 2009, *ApJ*, 703, 150
 Campana S., Mainetti D., Colpi M., Lodato G., D’Avanzo P., Evans P. A., Moretti A., 2015, *A&A*, 581, A17
 Cenko S. B. et al., 2012a, *MNRAS*, 420, 2684
 Cenko S. B. et al., 2016, *ApJ*, 818, L32
 Cenko S. B. et al., 2012b, *ApJ*, 753, 77
 Chen X., Madau P., Sesana A., Liu F. K., 2009, *ApJ*, 697, L149
 Chen X., Sesana A., Madau P., Liu F. K., 2011, *ApJ*, 729, 13
 Chornock R. et al., 2014, *ApJ*, 780, 44
 Cohen E., Piran T., 1999, *ApJ*, 518, 346
 Collin S., Zahn J.-P., 1999a, *A&A*, 344, 433
 Collin S., Zahn J.-P., 1999b, *Ap&SS*, 265, 501
 Comastri A. et al., 2002, *ApJ*, 571, 771
 Danforth C. W., Nalewajko K., France K., Keeney B. A., 2013, *ApJ*, 764, 57

⁴ <http://www.astro.washington.edu/users/jrad/idl.html>

⁵ <http://www.mrao.cam.ac.uk/~dag/CUBEHELIX/>

- Dolcini A. et al., 2005, *A&A*, 443, L33
- Dong S. et al., 2016, *Science*, 351, 257
- Dou L., Wang T., Yan L., Jiang N., Yang C., Cutri R. M., Mainzer A., Peng B., 2017, *ApJ*, 841, L8
- Dou L., Wang T.-g., Jiang N., Yang C., Lyu J., Zhou H., 2016, *ApJ*, 832, 188
- Drake A. J. et al., 2011, *ApJ*, 735, 106
- Dressler A., Gunn J. E., 1983, *ApJ*, 270, 7
- Eddington A. S., 1918, *ApJ*, 48, 205
- Eggen O. J., 1973, *ApJ*, 186, L1
- Elvis M., Schreier E. J., Tonry J., Davis M., Huchra J. P., 1981, *ApJ*, 246, 20
- Ferland G. J. et al., 2013, *Rev.Mex.AA*, 49, 137
- Fiore F. et al., 2003, *A&A*, 409, 79
- Frank J., Rees M. J., 1976, *MNRAS*, 176, 633
- French K. D., Arcavi I., Zabludoff A., 2016, *ApJ*, 818, L21
- Gal-Yam A., 2012, *Science*, 337, 927
- Gaskell C. M., Rojas Lobos P. A., 2014, *MNRAS*, 438, L36
- Generozov A., Mimica P., Metzger B. D., Stone N. C., Giannios D., Aloy M. A., 2017, *MNRAS*, 464, 2481
- Gezari S. et al., 2008, *ApJ*, 676, 944
- Gezari S., Chornock R., Lawrence A., Rest A., Jones D. O., Berger E., Challis P. M., Narayan G., 2015, *ApJ*, 815, L5
- Gezari S. et al., 2012, *Nature*, 485, 217
- Gezari S. et al., 2009, *ApJ*, 698, 1367
- Goel A., Maity R., Roy P., Sarkar T., 2015, *Phys. Rev. D*, 91, 104029
- Goto T., Kawai A., Shimono A., Sugai H., Yagi M., Hattori T., 2008, *MNRAS*, 386, 1355
- Goto T. et al., 2003, *PASJ*, 55, 771
- Green D. A., 2011, *Bulletin of the Astronomical Society of India*, 39, 289
- Griffiths R. E., Georgantopoulos I., Boyle B. J., Stewart G. C., Shanks T., della Ceca R., 1995, *MNRAS*, 275, 77
- Guillochon J., Manukian H., Ramirez-Ruiz E., 2014, *ApJ*, 783, 23
- Guillochon J., Ramirez-Ruiz E., 2013, *ApJ*, 767, 25
- Guillochon J., Ramirez-Ruiz E., 2015, *ApJ*, 809, 166
- Gurzadian V. G., Ozernoi L. M., 1981, *A&A*, 95, 39
- Hamers A. S., Perets H. B., 2017, *ApJ*, 846, 123
- Hills J. G., 1975, *Nature*, 254, 295
- Holoien T. W.-S. et al., 2016a, *MNRAS*, 463, 3813
- Holoien T. W.-S. et al., 2016b, *MNRAS*, 455, 2918
- Holoien T. W.-S. et al., 2014, *MNRAS*, 445, 3263
- Hung T. et al., 2017, *ApJ*, 842, 29
- Inserra C., et al., 2013, *ApJ*, 770, 128
- Ivanov P. B., Polnarev A. G., Saha P., 2005, *MNRAS*, 358, 1361
- Jaroszynski M., Abramowicz M. A., Paczynski B., 1980, *Acta Astron.*, 30, 1
- Jiang N., Dou L., Wang T., Yang C., Lyu J., Zhou H., 2016, *ApJ*, 828, L14
- Kaasra J. S. et al., 2014, *Science*, 345, 64
- Kaspi S., Maoz D., Netzer H., Peterson B. M., Vestergaard M., Jannuzi B. T., 2005, *ApJ*, 629, 61
- Kato M., Hōshi R., 1978, *Progress of Theoretical Physics*, 60, 1692
- Kewley L. J., Geller M. J., Barton E. J., 2006, *AJ*, 131, 2004
- Kim D.-W. et al., 2006, *ApJ*, 644, 829
- Kim S.-W., 2010, *Journal of Korean Physical Society*, 57, 673
- Komossa S., 2015, *Journal of High Energy Astrophysics*, 7, 148
- Komossa S. et al., 2009, *ApJ*, 701, 105
- Korista K. T., Goad M. R., 2004, *ApJ*, 606, 749
- Lacy J. H., Townes C. H., Hollenbach D. J., 1982, *ApJ*, 262, 120
- Laor A., 2003, *ApJ*, 590, 86
- Laor A., Fiore F., Elvis M., Wilkes B. J., McDowell J. C., 1997, *ApJ*, 477, 93
- Leloudas G. et al., 2016, *Nature Astronomy*, 1, 0002
- Levan A. J. et al., 2011, *Science*, 333, 199
- Lidskii V. V., Ozernoi L. M., 1979, *Soviet Astronomy Letters*, 5, 16
- Lodato G., King A. R., Pringle J. E., 2009, *MNRAS*, 392, 332
- Loeb A., Ulmer A., 1997, *ApJ*, 489, 573
- Luminet J.-P., Marck J.-A., 1985, *MNRAS*, 212, 57
- Magorrian J., Tremaine S., 1999, *MNRAS*, 309, 447
- Mathews W. G., Ferland G. J., 1987, *ApJ*, 323, 456
- McElroy R. E. et al., 2016, *A&A*, 593, L8
- Meliani Z., Vincent F. H., Grandclément P.,ourgoulhon E., Monceau-Baroux R., Straub O., 2015, *Classical and Quantum Gravity*, 32, 235022
- Metzger B. D., Stone N. C., 2016, *MNRAS*, 461, 948
- Miller J. M. et al., 2015, *Nature*, 526, 542
- Moriya T. J., Tanaka M., Morokuma T., Ohsuga K., 2017, *ApJ*, 843, L19
- Netzer H., 2013, *The Physics and Evolution of Active Galactic Nuclei*
- Oknyansky V. L. et al., 2016, *The Astronomer's Telegram*, 9015
- Ozernoi L. M., Reinhardt M., 1978, *Ap&SS*, 59, 171
- Perets H. B., Li Z., Lombardi, Jr. J. C., Milcarek, Jr. S. R., 2016, *ApJ*, 823, 113
- Piran T., Svirski G., Krolik J., Cheng R. M., Shiokawa H., 2015, *ApJ*, 806, 164
- Pracy M. B., Kuntschner H., Couch W. J., Blake C., Bekki K., Briggs F., 2009, *MNRAS*, 396, 1349
- Pracy M. B., Owers M. S., Zwaan M., Couch W., Kuntschner H., Croom S. M., Sadler E. M., 2014, *MNRAS*, 443, 388
- Quinlan G. D., 1996, *New Astronomy*, 1, 35
- Quintero A. D. et al., 2004, *ApJ*, 602, 190
- Rees M. J., 1988, *Nature*, 333, 523
- Renzini A., Greggio L., di Serego Alighieri S., Cappellari M., Burstein D., Bertola F., 1995, *Nature*, 378, 39
- Roth N., Kasen D., Guillochon J., Ramirez-Ruiz E., 2016, *ApJ*, 827, 3
- Ryu S. G., Nobukawa M., Nakashima S., Tsuru T. G., Koyama K., Uchiyama H., 2013, *PASJ*, 65, 33
- Sandrinelli A., Covino S., Treves A., 2014, *A&A*, 562, A79
- Saxton C. J., Soria R., Wu K., Kuin N. P. M., 2012, *MNRAS*, 422, 1625
- Saxton C. J., Younsi Z., Wu K., 2016, *MNRAS*, 461, 4295
- Saxton R. D., Motta S. E., Komossa S., Read A. M., 2015, *MNRAS*, 454, 2798
- Schwarzschild K., 1916, *Abh. Konigl. Preuss. Akad. Wissenschaften Jahre*, 1916, 189
- Severgnini P. et al., 2003, *A&A*, 406, 483
- Shappee B. J. et al., 2014, *ApJ*, 788, 48
- Sirko E., Goodman J., 2003, *MNRAS*, 341, 501
- Smith N. et al., 2015, *MNRAS*, 449, 1876
- Stone N. C., Metzger B. D., 2016, *MNRAS*, 455, 859
- Stone N. C., van Velzen S., 2016, *ApJ*, 825, L14
- Storchi-Bergmann T., Baldwin J. A., Wilson A. S., 1993, *ApJ*, 410, L11
- Strubbe L. E., Murray N., 2015, *MNRAS*, 454, 2321
- Strubbe L. E., Quataert E., 2009, *MNRAS*, 400, 2070
- Svirski G., Piran T., Krolik J., 2017, *MNRAS*, 467, 1426
- Tanaka T. L., 2013, *MNRAS*, 434, 2275
- Terlevich R., Tenorio-Tagle G., Franco J., Melnick J., 1992, *MNRAS*, 255, 713
- Tran H. D., 2001, *ApJ*, 554, L19
- Ulmer A., 1999, *ApJ*, 514, 180
- Ulrich M.-H., Maraschi L., Urry C. M., 1997, *ARA&A*, 35, 445
- van Velzen S., 2017, *ArXiv e-prints*, 1707.03458
- van Velzen S. et al., 2016a, *Science*, 351, 62
- van Velzen S. et al., 2011, *ApJ*, 741, 73
- van Velzen S., Frail D. A., Körding E., Falcke H., 2013, *A&A*, 552, A5
- van Velzen S., Körding E., Falcke H., 2011, *MNRAS*, 417, L51

- van Velzen S., Mendez A. J., Krolik J. H., Gorjian V., 2016b, *ApJ*, 829, 19
- Vasiliev E., 2014, *Classical and Quantum Gravity*, 31, 244002
- Vergani D. et al., 2010, *A&A*, 509, A42
- Verner D. A., Ferland G. J., 1996, *ApJS*, 103, 467
- Vreeswijk P. M., et al., 2014, *ApJ*, 797, 24
- Wang J., Merritt D., 2004, *ApJ*, 600, 149
- Wang T.-G., Zhou H.-Y., Wang L.-F., Lu H.-L., Xu D., 2011, *ApJ*, 740, 85
- Wegg C., Nate Bode J., 2011, *ApJ*, 738, L8
- Wevers T., van Velzen S., Jonker P. G., Stone N. C., Hung T., Onori F., Gezari S., Blagorodnova N., 2017, *MNRAS*, 471, 1694
- Wyrzykowski L. et al., 2017, *MNRAS*, 465, L114
- Xie G. Z., Liang E. W., Xie Z. H., Dai B. Z., 2002, *AJ*, 123, 2352
- Yamauchi C., Goto T., 2005, *MNRAS*, 359, 1557
- Yang Y., Tremonti C. A., Zabludoff A. I., Zaritsky D., 2006, *ApJ*, 646, L33
- Yang Y., Zabludoff A. I., Zaritsky D., Lauer T. R., Mihos J. C., 2004, *ApJ*, 607, 258
- Young P. J., Shields G. A., Wheeler J. C., 1977, *ApJ*, 212, 367
- Zabludoff A. I., Zaritsky D., Lin H., Tucker D., Hashimoto Y., Shectman S. A., Oemler A., Kirshner R. P., 1996, *ApJ*, 466, 104
- Zel'dovich Y. B., Raizer Y. P., 1967, *Physics of shock waves and high-temperature hydrodynamic phenomena*
- Zhang E.-P., Wang J.-M., 2006, *ApJ*, 653, 137

APPENDIX A: CURRENTLY IDENTIFIED UV/O TDE CANDIDATES

Table A1 provides a listing of currently identified TDE candidate events with spectral lines, including the transient previously identified by Drake et al. (2011) as a SN (but see Generozov et al. 2017 suggesting it is too luminous for a TDE, and Moriya et al. 2017 suggesting an AGN flare). Spectral types are labelled as: ‘He’ for He II-bright states; ‘He+H’ for both He II and H α emission; ‘H’ for H α -bright; and ‘abs’ for the absorption line comparison case. The clouds’ emission line characteristic velocity (v) is defined as in Arcavi et al. (2014). Where the observational papers give a bolometric luminosity (L), we use those values. Otherwise, we interpolate and estimate values from the published photometric light-curves. SMBH mass estimates are from the references. (Wevers et al. 2017 infer some smaller m_{\bullet} from host galaxy velocity dispersions, but we tabulate the older published values for the sake of consistency.)

Through dimensional analyses, it can be shown that the composite scores v^4/L and Lv^4/m_{\bullet} should be correlated with ionization parameter (if details of the system geometry were otherwise equal). In these terms, there seems to be a tendency for the H α -bright events to have lower scores than the He II-overbright events. It is however not a strong trend, and perhaps not statistically significant. We were unable to use Table A1 to declare any clear, quantitative predictor of the Arcavi et al. (2014) spectral sequence. In the Appendix B, we search for patterns and discriminants in a different way, under particular model assumptions.

APPENDIX B: OBSERVED VS EXPECTED VELOCITIES OF THE ILLUMINATED CLOUD

The presently available observations ought to appear more orderly under assumption of an event type: TDE or AGN flare. Empirically, the characteristic radius of a steady active galaxy’s BLR is $R_{\text{BLR}} \approx R_{44}(L/10^{44} \text{ erg s}^{-1})^A$ where an index $A = \frac{1}{2}$ is the ideal if the BLR size were constrained by a threshold temperature (e.g. of dust sublimation). From reverberation mapping in the 5100Å monochromatic luminosity λL_{λ} , Kaspi et al. (2005) find $R_{44} = 22.3 \pm 2.1$ light day and $A = 0.69 \pm 0.05$. Given this sizing, and SMBH mass estimates (Arcavi et al. 2014), we obtain a characteristic orbital velocity of the BLR clouds (v_k). If however the event were a TDE, then the stellar tidal disruption radius provides the relevant v_k estimator. Fig. B1 compares observed spectroscopic line widths (v_s) to the v_k estimates in both models. Assuming stars of solar density, the TDE scenario works poorly: the measured velocities are 0.02 to 0.2 times predicted, and the values seem uncorrelated with v_k ; and neither does the AGN model show any significant correlation. The measured velocities are a factor of a few higher than AGN expectations. From these simple scaling arguments, neither the TDE nor AGN scenarios fits the UV/O events impressively well, but the AGN version may seem somewhat less discordant. The weakness of the correlation between actual and expected velocities implies that the line-emitters are not causally related to the flaring event. Rather, we suppose that they were pre-existing, dormant circumnuclear clouds that revived and reactivated as a BLR when irradiated by the explosive event.

APPENDIX C: CLOUDY CALCULATIONS AND THE LINE RATIOS IN THE PHOTOIONIZATION CUBE PARAMETER PHASE SPACE

For each SED, we run several cubes of calculations: exploring a rectangle of ($N_{\text{H}}, n_{\text{H}}, \Phi_{\text{H}}$) in steps of 0.1 dex, and saving depth profiles along the N_{H} or spatial axis. We re-run extra cubes where the maximum column was set to $N_{\text{H}} = 10^{23}, 10^{24}, 10^{25} \text{ cm}^{-2}$. To allay concerns about the validity of CLOUDY’s approximate treatment of electron scattering, we conservatively exclude opaque models in our final results. The maximum N_{H} for every ($n_{\text{H}}, \Phi_{\text{H}}$) is manually adjusted to give a maximum optical depth of $\tau_{\text{es}} \leq 0.5$ (often near $N_{\text{H}} \approx 10^{23.8} \text{ cm}^{-2}$). From runs generated with different stopping columns, the coinciding parts of the line intensity vs depth profiles agree within an order of unity scale factor.

CLOUDY version 13.03 enables output of intensities from the illuminated face of the cloud, or the total of inward and outward faces. Unless otherwise stated, we use the inward face, which is most relevant for light-echo effects.

In every numerical run, CLOUDY reports the mean energy of a photoionizing photon (Average nu), the intensity of ionizing photons (I(nu>1ryd)), and the total intensity (Total inten). Using these, or numerical integration of the known SED function, provides a characteristic photon energy ($\bar{\epsilon}$, enabling conversion between the ionizing flux (Φ_{H} , user selected), an assumed cloud radial position (R_c), and the bolometric luminosity of the source (L). If L is known,

Table A1. Column 1: name of the TDE event or host. Column 2: type of broad line system: He-dominated emission; both HeII and H α emission; H α -dominated emission; absorption. Column 3: SMBH mass estimate. Column 4: time relative to peak luminosity. column 5: blackbody temperature (alternative versions for PS1-10jh). Column 6: photometry used ('-' marks bolometric estimates given by reference). Column 7: luminosity (derived from photometry if necessary). Column 8: velocity width of broad line. Column 9: ionization estimator. Column 10: ionization estimator using estimated m_{\bullet} . Column 11: references: (a) Gezari et al. 2012; (b) Arcavi et al. 2014; (c) Wang et al. 2011; (d) Holoien et al. 2014; (e) van Velzen et al. 2011; (f) Drake et al. 2011; (g) Chornock et al. 2014; (h) Miller et al. 2015; (i) Holoien et al. 2016b; (j) Holoien et al. 2016a; (k) Wyrzykowski et al. 2017; (l) Blagorodnova et al. 2017; (m) Hung et al. 2017.

object	type	m_{\bullet} ($10^6 m_{\odot}$)	t (day)	T_{bb} (10^4 K)	band	L ($10^9 L_{\odot}$)	v (10^3 km/s)	$\log\left(\frac{v^4}{L}\right)$	$\log\left(\frac{Lv^4}{m_{\bullet}^2}\right)$	ref.
PS1-10jh	He	4.0_{-2}^{+4}	-22	$\gtrsim 2.9 \pm 0.2$	$g_{P1} r_{P1} i_{P1}$	$\gtrsim 22.6 \pm 3$	5.43 ± 1.46	$\lesssim 1.6 \pm 1.1$	$\gtrsim 3.1_{-1.5}^{+2.3}$	a,b
PTF09ge	He	$5.65_{-0.98}^{+3.02}$	-18	2.1 ± 0.3	-	13.0 ± 4.6	10.07 ± 0.67	2.9 ± 0.4	$3.6_{-0.6}^{+1.2}$	b
SDSSJ0748	He+H	$11.78_{-3.56}^{+2.29}$	> 0	1.3 ± 0.4	g	$> 1.4 \pm 0.6$	9.95 ± 0.51	$< 3.8 \pm 0.5$	$> 2.0_{-0.8}^{+0.6}$	b,c
ASASSN-14ae	H	$2.45_{-0.74}^{+1.55}$	0	2.3 ± 0.1	V	38.3 ± 3.6	3.60 ± 0.18	0.6 ± 0.2	$3.0_{-0.6}^{+1.3}$	b,d
	H	..	4	2.1 ± 0.1	-	10.5 ± 0.4	7.2 ± 0.2	2.4 ± 0.1	$3.7_{-0.6}^{+1.3}$	
	H	..	30	1.6 ± 0.1	-	5.6 ± 0.4	6.0 ± 0.2	2.4 ± 0.2	$3.1_{-0.6}^{+1.3}$	
	H	..	51	1.6 ± 0.1	-	2.9 ± 0.2	5.1 ± 0.2	2.4 ± 0.2	$2.5_{-0.6}^{+1.3}$	
	H	..	73	2.1 ± 0.2	-	1.7 ± 0.2	4.2 ± 0.2	2.3 ± 0.2	$2.0_{-0.6}^{+1.3}$	
	He+H	..	94	2.1 ± 0.3	-	1.3 ± 0.3	3.4 ± 0.2	2.0 ± 0.3	$1.5_{-0.7}^{+1.3}$	
	He+H	..	132	2.0 ± 0.2	-	0.3 ± 0.2	3.4 ± 0.2	2.6 ± 0.6	$0.8_{-0.9}^{+1.4}$	
ASASSN-15oi	He	25.0_{-13}^{+25}	7	2.0 ± 0.4	-	52.0 ± 25	8.4 ± 0.4	2.0 ± 0.5	$2.6_{-1.1}^{+2.1}$	j
	He+H	..	21	7.5 ± 0.4	-	35.0 ± 17	3.9 ± 0.4	0.8 ± 0.6	$1.1_{-1.2}^{+2.1}$	
ASASSN-14li	He+H	3.0 ± 2	35	3.5 ± 0.4	-	83.2 ± 2.6	1.3 ± 0.4	-1.5 ± 1.3	1.4 ± 1.9	h,i
OGLE16aaa	He+H	$3.8_{-1.9}^{+3.8}$	-3	$\gtrsim 2.2$	I	86.0 ± 4	7.6 ± 0.4	1.6 ± 0.2	$4.3_{-1.0}^{+2.0}$	k
iPTF16fnl	He+H	6.3 ± 0.4	0	1.9 ± 0.2	-	2.6 ± 0.4	5.9 ± 0.4	2.7 ± 0.3	$2.9_{-0.7}^{+1.5}$	l
iPTF16axa	He+H	$5.0_{-2.9}^{+7.0}$	> 0	3.0 ± 0.33	-	$> 29.0 \pm 4$	4.0 ± 0.2	$< 1.0 \pm 0.2$	$> 2.5_{-1.2}^{+2.8}$	m
PTF09axc	H	$2.69_{-0.64}^{+0.66}$	≈ 5	1.2 ± 0.2	-	4.7 ± 2.4	11.89 ± 0.22	3.6 ± 0.5	4.1 ± 0.7	b
PTF09djl	H	$3.57_{-2.96}^{+9.97}$	2	2.6 ± 0.4	-	30.0 ± 14	6.53 ± 0.35	1.8 ± 0.5	$3.6_{-1.7}^{+5.6}$	b
		..	31	2.0 ± 0.3	-	15.0 ± 9	6.53 ± 0.35	2.1 ± 0.6	$3.3_{-1.7}^{+5.6}$	
		..	62	> 3.2	-	< 124	6.53 ± 0.35	$> 1.2 \pm 0.2$	$< 4.2_{-1.7}^{+5.6}$	
TDE2	H	$35.52_{-25.80}^{+55.31}$	> 40	1.82 ± 0.07	g	42.0 ± 2.9	3.44 ± 0.11	0.5 ± 1.3	$0.7_{-1.9}^{+3.4}$	b,e
CSS100217	H	$14.7_{-2.0}^{+2.4}$	-5	1.62 ± 0.18	V	439.0 ± 104	1.20 ± 0.04	-2.3 ± 0.3	0.6 ± 0.3	f
		..	20	1.35 ± 0.08	V	267.0 ± 36	1.36 ± 0.04	-1.9 ± 0.2	$0.6_{-0.3}^{+0.4}$	
		..	84	0.78 ± 0.20	V	67.0 ± 16	2.07 ± 0.04	-0.6 ± 0.3	0.6 ± 0.5	
		..	164		V	$< 4.6 \pm 1.1$	1.63 ± 0.04	$> 0.2 \pm 0.3$	$< -1.0 \pm 0.6$	
PS1-11af	abs	8.0 ± 2.0	24	1.7 ± 0.3	-	22.1 ± 0.5	4.31 ± 0.34	1.2 ± 0.3	1.9 ± 0.3	g

then we infer the distance between the source and the cloud,

$$R_c = \left[\frac{L}{4\pi\bar{\epsilon}\Phi_H} \right]^{1/2}. \quad (\text{C1})$$

The emission line luminosity (L_{λ}) and the cloud mass (M_c) depend on the cloud covering factor ($0 < \Omega < 1$) and the line's specific intensity (I_{line} , calculated by CLOUDY). Generally,

$$L_{\lambda} = 4\pi R_c^2 I_{\text{line}} \Omega = \frac{L}{\bar{\epsilon}\Phi_H} I_{\text{line}} \Omega \quad (\text{C2})$$

$$M_c = 4\pi R_c^2 \mu m_p N_H \Omega = \frac{L}{\bar{\epsilon}\Phi_H} \mu m_p N_H \Omega = \mu m_p \frac{L_{\lambda}}{I_{\text{line}}} N_H, \quad (\text{C3})$$

where μ is the mean molecular weight, and m_p is the proton mass. We can either make a fiducial assumption about the covering factor (e.g. $\Omega = 0.1$), or we can calculate a self-consistent value if both the line luminosity and continuum luminosity are known,

$$\Omega = \frac{L_{\lambda}}{L} \frac{\bar{\epsilon}\Phi_H}{I_{\text{line}}}. \quad (\text{C4})$$

In practice, Φ_H is a user-chosen runtime parameter; $\bar{\epsilon}$ is a

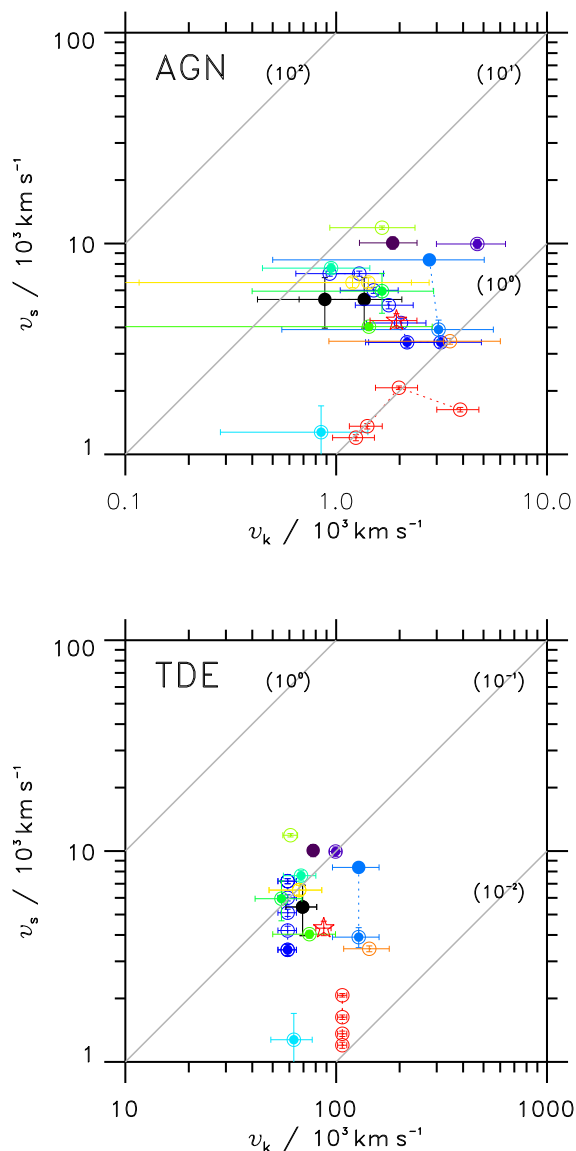


Figure B1. Comparison of observed velocity widths (v_s) with expected Keplerian velocity (v_k) estimated using scaling assumptions from AGN broad line regions (top) and TDE tidal radii (bottom). Guidelines mark the ratio v/v_k in powers of ten. Open circle symbols are events with H α emission; filled circles are events with He II emission; the starred event has broad absorption lines.

constant for each SED; I_{line} is output from CLOUDY for given $(N_{\text{H}}, n_{\text{H}}, \Phi_{\text{H}})$; L_{λ} is the observed line luminosity; and the total luminosity L is observationally inferred. Thus we assemble cubes of results in the $(N_{\text{H}}, n_{\text{H}}, \Phi_{\text{H}})$ parameter cube, and give them quantitative interpretation in the empirical context of a specific TDE candidate. Imposing some commonsense conditions can whittle the possibilities, to leave a set of physically reasonable results.

- For self-consistency, the clouds must be outside the opaque photosphere of the actively luminous source ($R_c > R_o$, where $L_o = 4\pi R_o^2 \sigma T_o^4$ for a blackbody sphere).

- Clouds can't cover more than the whole source ($\Omega < 1$).

- The He II/H α line ratio and the respective equivalent widths can be checked for consistency with observations.

Before interpreting the scale-independent CLOUDY results to model a particular TDE candidate event, a minority of the numerical output requires filtering for artifacts. For the hotter blackbody scenarios, a numerical instability sometimes occurs near the far end of the spatial grid. In these incidents, CLOUDY reports global non-convergence (which might have been the numerical problem reported by Strubbe & Murray 2015). On close inspection, the majority of the profile is however stable. We can retain these good sections, and excise the final 0.2 dex in N_{H} , and any unrealistically steep jumps in He II intensity. After this initial filtering, a smaller minority of numerical spikes remain; but their sensitivity to resolution proves their spuriousness. These glitches occur at uninterestingly low N_{H} , in configurations where the ionization parameter is low ($U < 0.03$), so from some cubes we exclude models with $\Phi_{\text{H}}/n_{\text{H}} < 10^9 \text{ cm s}^{-1}$.

The three-parameter cube of photoionization states in $(N_{\text{H}}, n_{\text{H}}, \Phi_{\text{H}})$ is conventionally visualized in terms of cross-sections: the constant- N_{H} flux-density planes (e.g. Korista & Goad 2004). For our purposes, in evaluating the possible conditions surrounding UV/O nuclear transients, it is more useful to project the non-linear surfaces to select N_{H} values that maximise the He II/H α line ratio at each $(n_{\text{H}}, \Phi_{\text{H}})$, to prioritise He II-bright events. Fig. C1 shows the results of coarse mapping of the local peak ratio for given $(n_{\text{H}}, \Phi_{\text{H}})$ pairs on a grid with 0.1dex steps on each axis, showing the effect of blackbody source SEDs. Top-left panels of each block show maximum line ratios at each $(n_{\text{H}}, \Phi_{\text{H}})$. He II-overbright states occupy the minority region appearing as a dark (green-blue) inclined ‘sausage.’ If these conditions are unmet, a cloud can only be a He II+H α or H α -dominated event. The lower two panels of each block show the equivalent widths W_{4686} and W_{6563} (assuming $\Omega = 0.1$) in the peak line ratio conditions. The top-right panels show the N_{H} values that gave each peak line ratio. He II-bright states require column densities near the highest we investigated. Echo models assume that the clouds were photoionized by an early, hard flash from a compact, hot blackbody. After the radiation-dominated ball expands and cools for some time, the observed continuum settles near $3 \times 10^4 \text{ K}$. The effect of the light-echo correction — early hard photoionization source superimposed on a later cooled continuum, according to the light crossing time — is to lower the equivalent widths.

This paper has been typeset from a $\text{\TeX}/\text{\LaTeX}$ file prepared by the author.

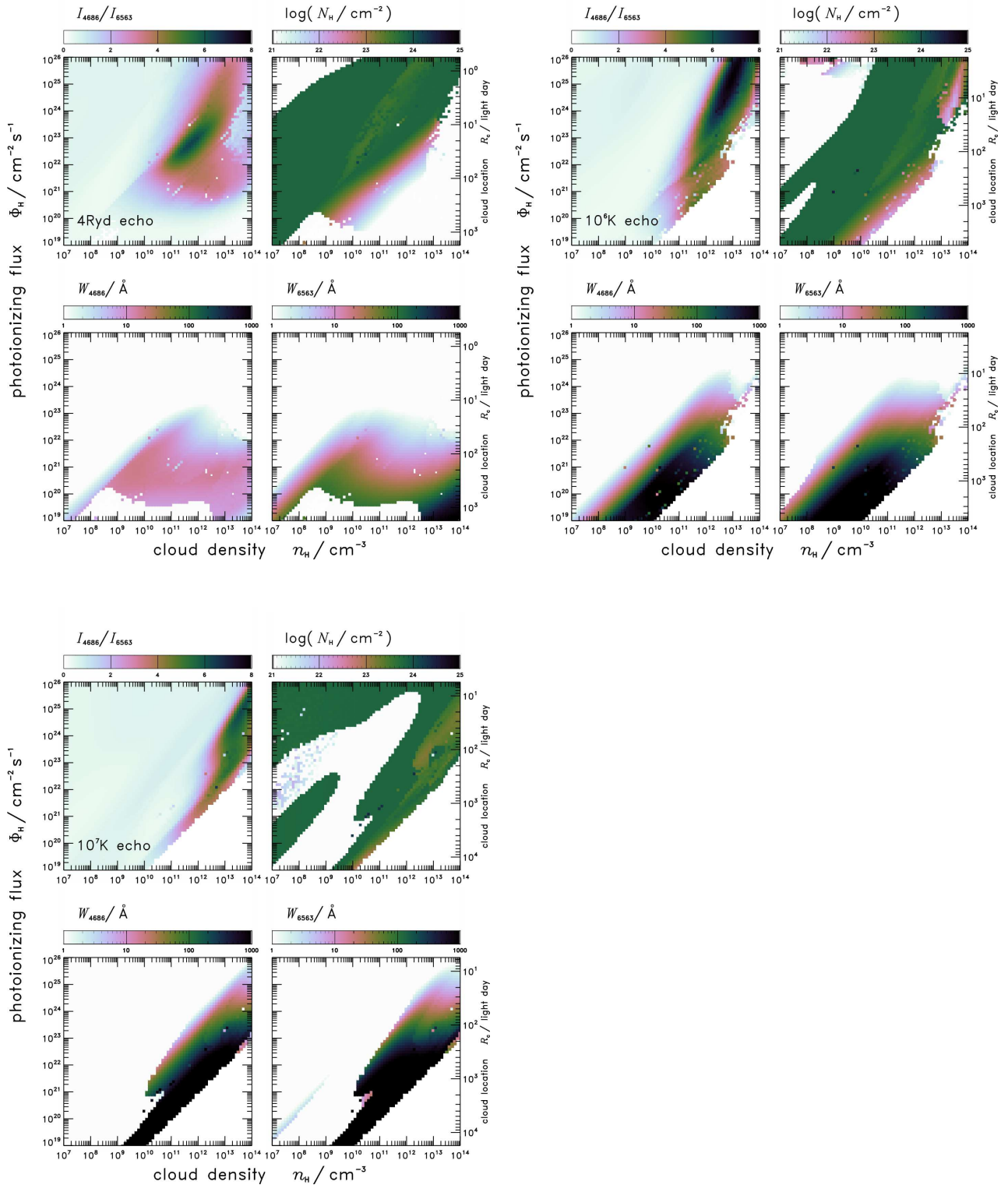


Figure C1. Conditions where N_{H} maximises the He II(4686Å) to H α (6563Å) intensity ratio, at given $(n_{\text{H}}, \Phi_{\text{H}})$. The equivalent widths derive from continuum estimates in a ‘light echo’ model, assuming that the currently visible continuum is a blackbody of $3 \times 10^4\text{K}$, and the earlier flash illuminating the clouds is a 4Ryd, 10^6K or 10^7K blackbody (first, second and third blocks respectively). These plots pertain to radation from the illuminated face of each cloud.